Case Studies in Construction Materials 19 (2023) e02406

Contents lists available at ScienceDirect

Case Studies in Construction Materials

journal homepage: www.elsevier.com/locate/cscm

Case study

Data-enabled comparison of six prediction models for concrete shrinkage and creep

Cole Shurbert-Hetzel [a], Dana Daneshvar [b], Agathe Robisson [b], Behrouz Shafei [a,*]

[a] Department of Civil, Construction, and Environmental Engineering, Iowa State University, Ames, IA 50011, United States
[b] Building Materials and Materials Technology, Department of Civil Engineering, Vienna University of Technology, Vienna, Austria

ARTICLE INFO

Keywords:
Concrete
Shrinkage
Creep
Predictive models
Input and output parameters
Data-assisted calibration

ABSTRACT

Modeling the shrinkage and creep of concrete is a demanding task due to the large number and high complexity of the parameters that contribute to these two mechanisms. A range of models have been developed to date to predict shrinkage and creep over time. Among them, this study focused on some of the most widely used models, including those developed by the American Association of State Highway and Transportation Officials, the American Concrete Institute, the European Committee for Standardization, the Fédération Internationale du Béton, and the Comité Européen du Béton. This holistic investigation aimed to provide in-depth insights into the input requirements and prediction capabilities of the identified models. For this purpose, using various data sets selected from the NU-ITI database, the performance of each shrinkage and creep model was first assessed, and a calibration approach was then employed to further refine their outputs. The calibration was performed with the objective of adjusting the short- and long-term prediction accuracy, including the rate of shrinkage and creep development over time. The models were evaluated side by side through comparing the outputs of each calibrated model to data from shrinkage and creep experiments. The calibration steps explored in this study were found to improve the performance of the shrinkage and creep prediction models by up to 20%. This helped reduce the possibility to deviate from the expected strains and stresses. The outcome of this detailed study paved the way to properly select and utilize shrinkage and creep models, taking into consideration the key contributing factors for the highest accuracy.

1. Introduction

Concrete is known to exhibit time-dependent deformations mainly due to shrinkage and creep. The effects of shrinkage and creep can directly impact the performance of concrete structures by the formation and propagation of cracks, redistribution of stresses, and loss of prestressing forces [1,2]. Such effects are pronounced particularly in situations that large deflections due to shrinkage and creep can cause various strength and serviceability issues [3–5]. Shrinkage and creep are, therefore, crucial factors in the design and analysis of concrete structures, especially for long-term performance. Shrinkage of concrete is a time-dependent process that results in volumetric contraction with the risk of generating cracks in the presence of constraints [6]. Various types of shrinkage are commonly observed in the concrete. Among them, autogenous shrinkage and drying shrinkage are the most critical types of shrinkage from a structural design and assessment standpoint [7]. Autogenous shrinkage is the macroscopic reduction in dimension under a constant

* Corresponding author.
E-mail address: shafei@iastate.edu (B. Shafei).

https://doi.org/10.1016/j.cscm.2023.e02406
Received 4 June 2023; Received in revised form 16 July 2023; Accepted 15 August 2023
Available online 19 August 2023

temperature without any moisture exchange with the environment [8]. It results from water consumption during the hydration reactions that reduce the overall relative humidity in the cementitious matrix (also referred to as self-desiccation), inducing stresses linked to capillary depression [9,10]. Autogenous shrinkage is most critical in the concrete mixtures that have a low water-to-binder ratio [11,12]. This type of shrinkage is prominent during the first month after casting the concrete since it is linked to the cement hydration process. Thus, 60–90% of the concrete's autogenous shrinkage commonly takes place within the first 28 days [7,13].

Drying shrinkage is the other main type of shrinkage that induces time-dependent volumetric changes. The volumetric changes are primarily caused by water evaporation from the concrete's pore spaces. Thus, the concrete's mixture properties (in terms of water-to-binder ratio and aggregate type, size, and shape), concrete's microstructure characteristics (in terms of porosity, pore size distribution, and the mean radius of capillary menisci), surrounding environmental conditions (in terms of relative humidity, temperature, and air flow), and exposed surface-to-volume ratio are among the key parameters to consider [14]. Drying shrinkage often continues over a much longer time period than autogenous shrinkage and is generally several times more significant than autogenous shrinkage in conventional concretes, resulting in various performance issues [15–17]. In unrestrained reinforced concrete (RC) members, drying shrinkage is known to cause stresses in such a way that the embedded steel reinforcement can experience compressive stresses, while the concrete can undergo tensile stresses. In restrained members, such as multi-layer concrete composites, the drying shrinkage induces tensile stresses in the restrained overlay, leading to shear (friction) and normal (delamination) stresses at the interface between the overlay and the substrate [18,19]. The formation of tensile stresses is critical since concrete is susceptible to cracking under tension [20]. The magnitude of such effects is dependent on the shape of the RC member, amount of embedded steel reinforcement, and intensity of mechanical and environmental stressors [21–23].

Creep is a time-dependent property of concrete, resulting in continuous deformations over time under sustained loads. Creep strain is stress-dependent, and thus, influenced by stress history. Specifically, the creep strain's magnitude increases as the stress increases. Under certain loading and structural configurations, creep can act as a stress relaxation mechanism. Creep is often quantified in one of two ways: creep coefficient or specific creep. The creep coefficient is the ratio of creep strain to elastic strain. On the other hand, specific creep, also known as creep compliance, is the total stress-dependent strain per unit stress. The two components of creep are basic creep and drying creep. Basic creep is the creep measured in a condition where drying is avoided. Specifically, this creep component can be determined based on the total strain of a sealed loaded specimen minus the instantaneous elastic strain caused by the external load and the strain due to the autogenous shrinkage [24]. Basic creep is considered a constitutive material property independent of geometry and environmental conditions [25]. When drying is allowed, drying creep also occurs and can be determined by subtracting the basic creep strain, the instantaneous elastic strain caused by the load, and the shrinkage strain from the total strain.

A range of models have been proposed in the literature to predict shrinkage and creep. Empirical and physical law models have both been used in codes and the practice. Overall, these models were established based on the fittings applied to various subsets of experimental test data. Compared to the empirical models, the physical law models (semi-empirical) are derived from physical theories, such as the microprestress solidification theory [26,27]. They can, therefore, be employed for complex shrinkage and creep situations after proper calibration. Such calibrations are, however, proven to be challenging, mainly due to the large number of variables that must be considered in the predictive models. Although progress has been made in modeling shrinkage and creep, past studies have reported overestimations and underestimations [28–30]. To improve prediction accuracy, emerging data-driven analysis approaches have been considered. Among them are deep learning models represented by convolutional neural networks [31,32], ensemble machine learning models [33], multiscale microstructure-based models [34], and multi-objective genetic programming-based models [35]. Despite the advances made through the data-driven models, such approaches often have a black-box nature and are too complex for the common use of civil engineers and concrete practitioners.

To address the outlined fundamental and practical issues, this study aimed to provide holistic insights into the most common shrinkage and creep models used for RC structures. To achieve this goal, the models developed by the American Association of State Highway and Transportation Officials (AASHTO) [36], American Concrete Institute (ACI 209) [37], Comité Européen du Béton (CEB MC90–99) [38], European Committee for Standardization (EN) Eurocode 2 (EC2) [39], Fédération Internationale du Béton/International Federation for Structural Concrete (fib Model Code 2010) [40], and Bazant-Baweja (B3 Model) [26] were systematically considered. Using various data sets selected from the NU-ITI database [41,42], the performance of each shrinkage and creep model was first assessed, and then a calibration approach was employed to further refine their outputs. The calibration was performed with the objective of adjusting the short- and long-term prediction capabilities of the identified shrinkage and creep models, including their rate of shrinkage/creep development over time. The shrinkage and creep models were evaluated side by side through comparing the outputs of each calibrated model to the data from shrinkage and creep experiments. The outcome of this holistic study provides in-depth insights into the performance of the most common concrete shrinkage and creep prediction models. Such insights ensure the proper selection and use of such models, depending on target applications.

2. Shrinkage and creep models

2.1. AASHTO model

The AASHTO shrinkage and creep models are empirical models that predict the shrinkage strain and creep coefficient of concrete as a function of time [36]. Shrinkage strain in the AASHTO model is predicted based on the concrete age, time of drying, relative humidity, volume-to-surface ratio, and compressive strength. Shrinkage strain according to the AASHTO model is calculated following Eq. (1).

Table 1
Correction factors for shrinkage strain in the AASHTO model.

Correction Factor	Name	Equation	Variables
k_s	Volume-to-surface ratio factor	$\left[\frac{t}{\frac{26e^{0.36(V/S)}+t}{\frac{t}{45+t}}}\right]\left[\frac{1064-94(V/S)}{923}\right]$	t = Time since the end of curing (day) V = Volume (in^3) S = Surface area (in^2)
k_{hs}	Humidity factor for shrinkage	$2.00 - 0.014H$	H = Relative humidity (%)
k_f	Concrete strength factor	$\frac{5}{1+f'_{ci}}$	f'_{ci} = Concrete compressive strength (ksi)
k_{td}	Time development factor	$\frac{t}{61-4f'_{ci}+t}$	t = Time since the end of curing (day) f'_{ci} = Concrete compressive strength (ksi)

Table 2
Correction factors for creep coefficient in the AASHTO model.

Correction Factor	Name	Equation	Variables
k_s	Volume-to-surface ratio factor	$\left[\frac{t}{\frac{26e^{0.36(V/S)}+t}{\frac{t}{45+t}}}\right]\left[\frac{1.80-1.77e^{-0.54(V/S)}}{2.587}\right]$	t = Time since loading (day) V = Volume (in^3) S = Surface area (in^2)
k_{hc}	Humidity factor for creep	$1.56 - 0.008H$	H = Relative humidity (%)
k_f	Concrete strength factor	$\frac{5}{1+f'_{ci}}$	f'_{ci} = Concrete compressive strength (ksi)
k_{td}	Time development factor	$\frac{t}{61-4f'_{ci}+t}$	t = Time since loading (day) f'_{ci} = Concrete compressive strength (ksi)

$$\varepsilon_{sh} = 0.48k_s k_{hs} k_f k_{td}(10^{-3}) \tag{1}$$

where ε_{sh} is the shrinkage strain as a function of time, and k_s, k_{hs}, k_f, and k_{td} are correction factors defined in Table 1.

The creep coefficient in the AASHTO model is predicted based on the concrete age, time of loading, relative humidity, volume-to-surface ratio, and compressive strength. The creep coefficient according to the AASHTO model is defined following Eq. (2).

$$\phi = 1.9k_s k_{hc} k_f k_{td} t_i^{-0.118} \tag{2}$$

where ϕ is the creep coefficient as a function of time, t_i, and k_s, k_{hc}, k_f, and k_{td} are correction factors defined in Table 2.

The AASHTO shrinkage and creep models are among the simplest models available in the literature. This is partly because the models are primarily intended for use on a specific set of structures (i.e., bridges) with regulated concrete mixtures, curing regimes, and overall geometries. Under the conditions that the models are intended (e.g., for concretes with compressive strengths of up to 15 ksi (103.4 MPa), including minimum and maximum reinforcement thresholds), the AASHTO models can quickly provide shrinkage and creep values. However, if conditions differ from what the models are geared toward, they likely provide inaccurate predictions. The AASHTO models lack constants with a recommended value and/or range to tune them so that they can be fitted to experimental and/or field data. However, the models can easily be tuned to match long-term shrinkage and creep behavior by introducing factors into shrinkage strain and creep coefficient equations.

2.2. ACI 209 model

The ACI 209 shrinkage and creep models are empirical models that predict the shrinkage strain and creep coefficient of the concrete as a function of time [25,37]. Shrinkage strain is predicted based on the concrete age, curing method (moist or steam curing), time of drying, relative humidity, volume-to-surface ratio, slump, fine aggregate to total aggregate ratio, cement content, and air content. Shrinkage strain according to the ACI 209 model is calculated following Eq. (3).

$$\varepsilon_{sh}(t, t_c) = \frac{(t - t_c)^{\alpha}}{f + (t - t_c)^{\alpha}} \varepsilon_{shu} \tag{3}$$

where $\varepsilon_{sh}(t, t_c)$ is the shrinkage strain at a concrete age of t (in days), t_c is the concrete age at the time when drying starts (in days), α is a constant between 0.90 and 1.10 to tune the model to experimental test and/or field data, f is a constant between 20 and 130 days to tune the model further, and ε_{shu} is the ultimate shrinkage strain. The ultimate shrinkage strain, ε_{shu}, is defined according to Eqs. (4) and (5).

$$\varepsilon_{shu} = 780\gamma_{sh}(10^{-6}) \tag{4}$$

Table 3
Correction factors for shrinkage strain in the ACI 209 model.

Correction Factor	Name	Equation	Variables
$\gamma_{sh,tc}$	Initial moist curing coefficient	$1.202 - 0.2337\log(t_c)$	t_c = Moist curing duration (day)
$\gamma_{sh,RH}$	Ambient relative humidity coefficient	$1.40 - 1.02h$ for $0.40 \le h \le 0.800$ $3.00 - 3.0h$ for $0.80 \le h \le 1.00$	h = Relative humidity (decimal)
$\gamma_{sh,vs}$	Member size factor	$1.2e^{\left\{-0.12\left(\frac{V}{S}\right)\right\}}$	V = Volume (in^3) S = Surface area (in^2)
$\gamma_{sh,s}$	Slump factor	$0.89 + 0.041s$	s = Slump (inch)
$\gamma_{sh,\psi}$	Fine aggregate factor	$0.30 + 0.014\psi$ for $\psi \le 50\%$ $0.90 + 0.002\psi$ for $\psi > 100\%$	Ψ = Ratio of fine aggregate weight to total aggregate weight (%)
$\gamma_{sh,c}$	Cement content factor	$0.75 + 0.00036c$	c = Cement content (lb/yd^3)
$\gamma_{sh,\alpha}$	Air content factor	$0.95 + 0.008\alpha \ge 1.0$	α = Air content (%)

Table 4
Correction factors for creep coefficient in the ACI 209 model.

Correction Factor	Name	Equation	Variables
$\gamma_{c,to}$	Age of loading factor	$1.25{t_0}^{-0.118}$ for moist curing $1.13{t_0}^{-0.094}$ for steam curing	t_0 = Load applied (day)
$\gamma_{c,RH}$	Ambient relative humidity coefficient	$1.27 - 0.67h$ for $h \ge 0.40$	h = Relative humidity (decimal)
$\gamma_{c,vs}$	Member size factor	$\frac{2}{3}\left(1 + 1.13e^{\left\{-0.54\left(\frac{V}{S}\right)\right\}}\right)$	V = Volume (in^3) S = Surface area (in^2)
$\gamma_{c,s}$	Slump factor	$0.82 + 0.067s$	s = Slump (inch)
$\gamma_{c,\psi}$	Fine aggregate factor	$0.88 + 0.0024\psi$	Ψ = Ratio of fine aggregate weight to total aggregate weight (%)
$\gamma_{c,\alpha}$	Air content factor	$0.46 + 0.09\alpha \ge 1.0$	α = Air content (%)

$$\gamma_{sh} = \gamma_{sh,tc}\gamma_{sh,RH}\gamma_{sh,vs}\gamma_{sh,s}\gamma_{sh,\psi}\gamma_{sh,c}\gamma_{sh,\alpha} \tag{5}$$

where γ_{sh} is a product of a series of correction factors. The correction factors included in Eq. (5) for the ultimate shrinkage strain have been summarized in Table 3.

In the ACI 209 model, the creep coefficient is predicted based on the concrete age, curing method, time of loading, relative humidity, volume-to-surface ratio, slump, fine aggregate to total aggregate ratio, and air content. The creep coefficient at any time is estimated according to Eq. (6).

$$\phi(t, t_0) = \frac{(t - t_0)^{\Psi}}{d + (t - t_0)^{\Psi}}\phi_u \tag{6}$$

where $\phi(t, t_0)$ is the creep coefficient at the concrete age of t (in days), t_0 is the concrete age at the time of loading (in days), ψ is a constant between 0.40 and 0.80 to tune the model to experimental test and/or field data, d is a constant between 6 and 30 days to tune the model further, and ϕ_u is the ultimate creep coefficient. The ultimate creep coefficient is defined according to Eqs. (7) and (8).

$$\phi_u = 2.35\gamma_c \tag{7}$$

$$\gamma_c = \gamma_{c,to}\gamma_{c,RH}\gamma_{c,vs}\gamma_{c,s}\gamma_{c,\psi}\gamma_{c,\alpha} \tag{8}$$

where γ_c is the product of a series of correction factors for the ultimate creep coefficient. These correction factors for the ultimate creep coefficient have been summarized in Table 4.

A significant benefit of the ACI 209 models is their relative simplicity while yet allowing tuning to available data. For example, the α, f, ψ, and d constants from Eqs. (3) and (6) can be tuned to capture the shape of the shrinkage strain and creep coefficient curves. Additional factors can be applied to the ultimate shrinkage strain and ultimate creep coefficient to modify the ultimate values. Such features allow the models to accurately match nearly any set of data. The models also provide recommended ranges for all the constants, ultimate shrinkage strain, and ultimate creep coefficient to ensure an accurate estimate is obtained.

2.3. B3 model

The Bazant-Baweja (B3) model is a hybrid of empirical and theoretical models that predict the shrinkage strain and creep compliance of concrete as a function of time [26]. This model provides ultimate values of shrinkage strain and creep compliance, while distinguishing between the basic and drying components of creep. Shrinkage strain in this model is predicted based on the concrete age, curing method, time of drying, relative humidity, concrete strength, cement type, water content, cross-section shape, and volume-to-surface ratio. Shrinkage strain according to the B3 model is defined following Eq. (9).

Table 5
Factors and constants for shrinkage strain in the B3 model.

Correction Factor	Equation	Variables
k_h	$1-h^3$ for $h \le 0.98$ -0.2 for $h = 1.00$ $12.74-12.94h$ for $0.98 < h < 1.00$	h = Relative humidity (decimal)
$\varepsilon_{s\infty}$	$\alpha_1\alpha_2\left[0.02565w^{2.1}{f_{cm28}}^{-0.28}+270\right]\left(10^{-6}\right)$	w = Water content (lb/yd^3) f_{cm28} = Concrete compressive strength at 28 days (psi)
α_1	1.00 for Type I cement 0.85 for Type II cement 1.10 for Type III cement	–
α_2	0.75 for steam cured 1.00 for cured in water 1.20 for sealed curing	–
$E_{cm(t)}$	$E_{cm(28)}\left(\frac{t}{4+0.85t}\right)^{0.5}$	$E_{cm(28)}$ = Modulus of elasticity at 28 days (psi) t = Age of concrete (day)
k_s	1.00 for infinite slab 1.15 for infinite cylinder 1.25 for infinite square prism 1.30 for sphere 1.55 for cube	–

Table 6
Factors and constants for creep compliance in the B3 model.

Correction Factor	Equation	Variables
q_1	$0.6/E_{cm28}$	E_{cm28} = Modulus of elasticity at 28 days (psi)
q_2	$86.814(10^{-6}){c}^{0.5}{f_{cm28}}^{-0.9}$	c = Cement content (lb/yd^3) f_{cm28} = Mean concrete compressive strength at 28 days (psi)
q_3	$0.29(w/c)^4 q_2$	w/c = Water-to-cement ratio
q_4	$0.14(10^{-6})(a/c)^{-0.7}$	a/c = Aggregate-to-cement ratio
q_5	$0.757{f_{cm28}}^{-1}\lvert\varepsilon_{s\infty}(10^6)\rvert^{-0.6}$	f_{cm28} = Mean concrete compressive strength at 28 days (psi) $\varepsilon_{s\infty}$ = Factor from the shrinkage model
$Q(t,t_0)$	$Q_f(t_0)\left[1+\left(\frac{Q_f(t_0)}{Z(t,t_0)}\right)^{r(t_0)}\right]^{-1/r(t_0)}$	$Q_f(t_0)$ = Defined below. $Z(t,t_0)$ = Defined below. $r(t_0)$ = Defined below.
$Q_f(t_0)$	$\left[0.086(t_0)^{\frac{2}{9}}+1.21(t_0)^{\frac{4}{9}}\right]^{-1}$	t_0 = Age of loading (day)
$Z(t,t_0)$	$(t_0)^{-m}\ln[1+(t-t_0)^n]$	t_0 = Age of loading (day) $m = 0.5$ $n = 0.1$
$r(t_0)$	$1.7(t_0)^{0.12}+8$	t_0 = Age of loading (day)

$$\varepsilon_{sh}(t,t_c) = \varepsilon_{sh\infty}k_h S(t-t_c) \tag{9}$$

where $\varepsilon_{sh}(t,t_c)$ is the shrinkage strain at the concrete age of t (in days), t_c is the concrete age at the start of drying (in days), $\varepsilon_{sh\infty}$ is the ultimate shrinkage strain, k_h is a humidity dependence factor as defined in Table 5, and $S(t-t_c)$ is the time curve. The time curve is calculated following Eqs. (10) and (11).

$$S(t-t_c) = \tanh\sqrt{\frac{(t-t_c)}{\tau_{sh}}} \tag{10}$$

$$\tau_{sh} = 190.8{t_c}^{-0.08}{f_{cm28}}^{-0.25}[2k_s(V/S)]^2 \tag{11}$$

where τ_{sh} is the shrinkage half-time (in days), f_{cm28} is the concrete mean compressive strength at 28 days, k_s is a factor to account for the member shape as defined in Table 5, and V/S is the volume-to-surface ratio. The ultimate shrinkage strain is defined according to Eq. (12).

$$\varepsilon_{sh\infty} = \varepsilon_{s\infty}\frac{E_{cm(607)}}{E_{cm(t_c+\tau_{sh})}} \tag{12}$$

where $\varepsilon_{s\infty}$ is a constant as defined in Table 5, and $E_{cm(607)}$ and $E_{cm(t_c+\tau_{sh})}$ are the elastic moduli at their corresponding times, as defined in Table 5.

Creep compliance in the B3 model is predicted based on the concrete age, curing method, time of drying, time of loading, compressive strength, relative humidity, cement content, water-to-cement ratio, aggregate-to-cement ratio, cross-section shape, and

Table 7
Factors and constants for shrinkage strain in the CEB model.

Correction Factor	Equation				Variables
$\varepsilon_{caso}(f_{cm28})$	$-\alpha_{as}\left(\frac{f_{cm28}}{6+\frac{f_{cm28}}{f_{cmo}}}\right)^{2.5}(10^{-6})$				α_{as} = Defined below. f_{cmo} = 1450 psi f_{cm28} = Mean concrete compressive strength at 28 days (psi)
$\varepsilon_{cdso}(f_{cm28})$	$\left[(220+110\alpha_{ds1})e^{-\alpha_{ds2}f_{cm28}/f_{cmo}}\right](10^{-6})$				α_{ds1} = Defined below. α_{ds2} = Defined below. f_{cmo} = 1450 psi f_{cm28} = Mean concrete compressive strength at 28 days (psi)
α_{as}, α_{ds1}, α_{ds2}	Cement	α_{as}	α_{ds1}	α_{ds2}	–
	SL	800	3	0.13	
	N or R	700	4	0.12	
	RS	600	6	0.12	
$\beta_{as}(t)$	$1-e^{\left[-0.2\left(\frac{t}{t_1}\right)^{0.5}\right]}$				t = Age of concrete (day) t_1 = 1 day
$\beta_{RH}(h)$	$-1.55\left[1-\left(\frac{h}{h_0}\right)^3\right]$ for $0.4 \le h < 0.99$ 0.25 for $h \ge 0.99$				h = Relative humidity (decimal) h_0 = 1.0 β_{s1} = Defined below.
β_{s1}	$\left(\frac{3.5f_{cmo}}{f_{cm28}}\right)^{0.1} \le 1.0$				f_{cmo} = 1450 psi f_{cm28} = Mean concrete compressive strength at 28 days (psi)

volume-to-surface ratio. Creep compliance according to the B3 model is defined following Eq. (13).

$$J(t,t_0) = q_1 + C_0(t,t_0) + C_d(t,t_0,t_c) \tag{13}$$

where $J(t,t_0)$ is the creep compliance at the concrete age of t (in days), t_0 is the time of loading (in days), q_1 is a constant defined in Table 6, $C_0(t,t_0)$ is to account for basic creep, and $C_d(t,t_0,t_c)$ is to account for drying creep. $C_0(t,t_0)$ and $C_d(t,t_0,t_c)$ are defined according to Eqs. (14) and (15), respectively.

$$C_0(t,t_0) = q_2Q(t,t_0) + q_3\ln[1+(t-t_0)^n] + q_4\ln(t/t_0) \tag{14}$$

$$C_d(t,t_0,t_c) = q_5\left[e^{-8H(t)} - e^{-8H(t_0)}\right]^{1/2} \tag{15}$$

As presented in Table 6, the multiplying functions, i.e., q_2, q_3, and q_4, represent the nondimensionalized forms of the aging viscoelastic compliance, nonaging viscoelastic compliance, and flow compliance, respectively. Function $Q(t,t_0)$ can be calculated from an approximate explicit formula presented in Table 6. The empirical parameter n is taken as 0.1, and $H(t)$ and $H(t_0)$ are spatial averages of pore relative humidity, which can be obtained from Eqs. (16) through (19).

$$H(t) = 1-(1-h)S(t-t_c) \tag{16}$$

$$H(t_0) = 1-(1-h)S(t_0-t_c) \tag{17}$$

$$S(t-t_c) = \tanh\sqrt{\left(\frac{t-t_c}{\tau_{sh}}\right)^{1/2}} \tag{18}$$

$$S(t_0-t_c) = \tanh\sqrt{\left(\frac{t_0-t_c}{\tau_{sh}}\right)^{1/2}} \tag{19}$$

where h is the relative humidity, $S(t-t_c)$ and $S(t_0-t_c)$ are time curves, and τ_{sh} is the shrinkage half-time (in days).

The B3 models offer advantages due to their ties to theory. For example, basic and drying creep, as well as specific components of shrinkage, are calculated separately. Additionally, the B3 models are well suited for general use over a wide range of parameters that can affect shrinkage and creep. However, the B3 models do not provide a significant advantage over simple empirical models when calibrating a model to experimental test and/or field data. The models are also relatively complex, especially in comparison to the ACI 209 or AASHTO shrinkage and creep models.

2.4. CEB model

The CEB MC90–99 offers empirical shrinkage and creep models that predict the shrinkage strain and creep compliance of concrete, respectively, as a function of time [38]. Similar to the B3 model, the CEB model differentiates between autogenous and drying shrinkage. Additionally, the creep compliance function is calculated from a creep coefficient. Shrinkage strain in this model is predicted based on the concrete age, time of drying, relative humidity, volume-to-surface ratio, cement type, and compressive strength.

Table 8
Factors and constants for creep compliance in the CEB model.

Correction Factor	Equation	Variables
ϕ_0	$\phi_{RH}(h)\beta(f_{cm28})\beta(t_0)$	$\phi_{RH}(h)$ = Defined below. $\beta(f_{cm28})$ = Defined below. $\beta(t_0)$ = Defined below.
$\phi_{RH}(h)$	$\left[1+\frac{1-h/h_0}{\sqrt[3]{0.1[(V/S)/(V/S)_0]}}\alpha_1\right]\alpha_2$	h = Relative humidity (decimal) h_0 = 1.0 (V/S) = Volume-to-surface ratio (in) $(V/S)_0$ = 2 in. α_1 = Defined below. α_2 = Defined below.
α_1	$\left[\frac{3.5f_{cmo}}{f_{cm28}}\right]^{0.7}$	f_{cmo} = 1450 psi f_{cm28} = Mean concrete compressive strength at 28 days (psi)
α_2	$\left[\frac{3.5f_{cmo}}{f_{cm28}}\right]^{0.2}$	
α_3	$\sqrt{\frac{3.5f_{cmo}}{f_{cm28}}}$	
$\beta(f_{cm28})$	$\frac{5.3}{\sqrt{f_{cm28}/f_{cmo}}}$	f_{cm28} = Mean concrete compressive strength at 28 days (psi)
$\beta(t_0)$	$\frac{1}{0.1+(t_0/t_1)}$	t_0 = Age of concrete at loading (day) t_1 = 1 day
β_H	$150\left[1+\left(\frac{1.2h}{h_0}\right)^{18}\right]\frac{(V/S)}{(V/S)_0}+250\alpha_3 \le 1500\alpha_3$	h = Relative humidity (decimal) h_0 = 1.0 (V/S) = Volume-to-surface ratio (in) $(V/S)_0$ = 2 in. α_3 = Defined below.

Shrinkage strain according to the CEB model is defined following Eq. (20).

$$\varepsilon_{sh}(t,t_c)=\varepsilon_{cas}(t)+\varepsilon_{cds}(t,t_c) \tag{20}$$

where $\varepsilon_{sh}(t,t_c)$ is the total shrinkage at the concrete age of t (in days), t_c is the concrete age at the start of drying (in days), $\varepsilon_{cas}(t)$ is the autogenous component of shrinkage, and $\varepsilon_{cds}(t,t_c)$ is the drying component of shrinkage. The autogenous component of shrinkage is defined according to Eqs. (21) and (22).

$$\varepsilon_{cas}(t)=\varepsilon_{caso}(f_{cm28})\beta_{as}(t) \tag{21}$$

$$\beta_{as}(t)=1-e^{\left[-0.2\left(\frac{t}{t_1}\right)^{0.5}\right]} \tag{22}$$

where $\varepsilon_{caso}(f_{cm28})$ is the notional autogenous shrinkage coefficient defined in Table 7, $\beta_{as}(t)$ is the time development factor for autogenous shrinkage, and t_1 is equal to one day. The drying component of shrinkage is defined according to Eqs. (23) and (24).

$$\varepsilon_{cds}(t,t_c)=\varepsilon_{cdso}(f_{cm28})\beta_{RH}(h)\beta_{ds}(t-t_c) \tag{23}$$

$$\beta_{ds}(t-t_c)=\sqrt{\frac{(t-t_c)/t_1}{350\left[(V/S)/(V/S)_0\right]^2+((t-t_c)/t_1)}} \tag{24}$$

where $\varepsilon_{cdso}(f_{cm28})$ is the notional drying shrinkage coefficient defined in Table 7, $\beta_{RH}(h)$ is to account for relative humidity as defined in Table 7, $\beta_{ds}(t-t_c)$ is the time development factor for drying shrinkage, V/S is the volume-to-surface ratio, and $(V/S)_0$ is 2 in. (5.08 cm).

Creep compliance in the CEB model is predicted based on the concrete age, time of loading, relative humidity, volume-to-surface ratio, cement type, and compressive strength. Creep compliance according to the CEB model is defined following Eq. (25).

$$J(t,t_0)=\frac{1}{E_{cm28}}[\eta(t_0)+\phi_{28}(t,t_0)]=\frac{1}{E_{cmto}}+\frac{\phi_{28}(t,t_0)}{E_{cm28}} \tag{25}$$

where $J(t,t_0)$ is the creep compliance at the concrete age of t (in days), t_0 is the time of loading (in days), E_{cm28} is the modulus of elasticity at the age of 28 days (in psi), E_{cmto} is the modulus of elasticity at the time of loading (in psi), $\eta(t_0)$ is the ratio of E_{cm28} to E_{cmto}, and $\phi_{28}(t,t_0)$ is the 28-day creep coefficient. The 28-day creep coefficient is calculated according to Eqs. (26) and (27).

$$\phi_{28}(t,t_0)=\phi_0\beta_c(t-t_0) \tag{26}$$

Table 9
Factors and constants for shrinkage strain in the EC2 model.

Correction Factor	Equation	Variables
h_0	$\frac{2A_c}{(u)}$	A_c = Cross-sectional area u = Perimeter of the member in contact with atmosphere
k_h	1.0 for $h_0 = 100$ 0.85 for $h_0 = 200$ 0.75 for $h_0 = 300$ 0.70 for $500 \leq h_0$	h_0 = Defined above.
$\beta_{ds}(t, t_s)$	$\left(\frac{(t-t_s)}{(t-t_s)+0.04\sqrt[3]{h_0}}\right)$	h_0 = Defined above.
$\varepsilon_{cd,0}$ (f_{cm28}, RH)	$0.85((220+110\alpha_{ds1})\exp\left(-\alpha_{ds2}\frac{f_{cm28}}{f_{cmo}}\right))(10^{-6})\beta_{RH}$	α_{ds1} and α_{ds2} = Defined below. β_{RH} = Defined below. f_{cm28} = Mean concrete compressive strength at 28 days (MPa) f_{cmo} = 10 MPa
β_{RH}	$1.55(1-\left(\frac{RH}{RH_0}\right)^3)$	RH = Relative humidity (%) RH_0 = 100%
α_{ds1}	3 for cement class S 4 for cement class N 6 for cement class R	–
α_{ds2}	0.13 for cement class S 0.12 for cement class N 0.11 for cement class R	–
$\varepsilon_{ca,\infty}$(f_{ck28})	$2.5[f_{ck28}-10](10^{-6})$	f_{ck28} = Characteristic concrete compressive strength at 28 days (MPa)
$\beta_{as}(t)$	$1-\exp(-0.2t^{0.5})$	–

$$\beta_c(t-t_0) = \left[\frac{(t-t_0)/t_1}{\beta_H + (t-t_0)/t_1}\right]^{0.3} \tag{27}$$

where ϕ_0 is the notional creep coefficient, $\beta_c(t-t_0)$ is a coefficient that accounts for the time development of creep, and β_H accounts for relative humidity as defined in Table 8. Similar to the B3 model, the CEB model differentiates between basic and drying creep. The CEB model also allows for modifications to capture unusual temperatures and stress levels.

2.5. EC2 model

The EC2 proposes two approaches to predict shrinkage and creep [39]. First is a simplified approach to estimate time-dependent deformations where high accuracy is not required. The shrinkage and creep coefficients are extracted from empirical graphs and tables mainly based on the concrete strength class, humidity, nominal size, and type of cement. In the second approach, which provides improved accuracy, a set of equations to determine the drying shrinkage strain and creep coefficient are presented as a function of time, similar to the other presented models. Shrinkage strain in the detailed model is predicted based on the concrete age, time of drying, relative humidity, volume-to-surface ratio, cement type, compressive strength, and temperature. Shrinkage strain according to the EC2 model is defined following Eq. (28).

$$\varepsilon_{cs}(t, t_s) = \varepsilon_{cd}(t, t_s) + \varepsilon_{ca}(t) \tag{28}$$

where $\varepsilon_{cs}(t, t_s)$ is the total shrinkage at the concrete age of t (in days), t_s is the concrete age at the beginning of drying (in days), $\varepsilon_{cd}(t, t_s)$ is the drying component of shrinkage, and $\varepsilon_{ca}(t)$ is the autogenous component of shrinkage. The drying component of shrinkage is calculated according to Eqs. (29) and (30).

$$\varepsilon_{cd}(t, t_s) = \varepsilon_{cd,0}(f_{cm28}, RH)k_h\beta_{ds}(t, t_s) \tag{29}$$

$$\beta_{ds}(t, t_s) = \left(\frac{(t-t_s)}{(t-t_s)+0.04\sqrt[3]{h_0}}\right) \tag{30}$$

where $\varepsilon_{cd,0}(f_{cm28}, RH)$ is the basic drying shrinkage coefficient defined in Table 9, $\beta_{ds}(t, t_s)$ is the time development factor for drying shrinkage, and h_0 is the notional size of the cross-section defined in Table 9. The autogenous component of shrinkage is defined according to Eqs. (31) and (32).

$$\varepsilon_{ca}(t) = \varepsilon_{ca,\infty}(f_{ck28})\beta_{as}(t) \tag{31}$$

$$\beta_{as}(t) = 1 - e^{\left[-0.2(t)^{0.5}\right]} \tag{32}$$

where $\varepsilon_{ca,\infty}(f_{ck})$ is the notional autogenous shrinkage coefficient defined in Table 9, $\beta_{as}(t)$ is the time development factor for autogenous shrinkage, and f_{ck} is the characteristic compressive strength of the concrete.

Table 10
Factors and constants for creep compliance in the EC2 model.

Correction Factor	Equation	Variables
φ_{RH}	$1+\frac{1-RH/100}{0.1\sqrt[3]{h_0}}$ for $f_{cm} \le 35$MPa $\left(1+\frac{1-\frac{RH}{100}}{0.1\sqrt[3]{h_0}}\alpha_1\right)\alpha_2$ for $f_{cm} > 35$MPa	RH = Relative humidity (%) h_0 = Defined below.
$\beta(f_{cm28})$	$\frac{16.8}{\sqrt{f_{cm28}}}$	f_{cm28} = Mean concrete compressive strength at 28 days (MPa)
$\beta(t_0)$	$\frac{1}{(0.1+t_0{}^{0.2})}$	t_0 = Age of concrete at loading (day)
h_0	$\frac{2A_c}{(u)}$	A_c = Cross-sectional area u = Perimeter of the member in contact with atmosphere
$\beta_c(t,t_0)$	$\left(\frac{(t-t_0)}{\beta_H+t-t_0}\right)^3$	$t-t_0$ = Non-adjusted duration of loading (day) β_H = Coefficient of relative humidity and notional member size
β_H	$1.5(1+(0.012RH)^{18})h_0+250 \le 1500$ for $f_{cm} \le 35$ MPa $1.5(1+(0.012RH)^{18})h_0+250\alpha_3 \le 1500$ for $f_{cm} > 35$ MPa	RH = Relative humidity (%)
α_1	$\left(\frac{35}{f_{cm28}}\right)^{0.7}$	f_{cm28} = Mean concrete compressive strength at 28 days (MPa)
α_2	$\left(\frac{35}{f_{cm28}}\right)^{0.2}$	
α_3	$\left(\frac{35}{f_{cm28}}\right)^{0.5}$	

Table 11
Factors and constants for shrinkage strain in the fib model.

Correction Factor	Equation	Variables
$\varepsilon_{cbs0}(f_{cm28})$	$-\alpha_{bs}\left(\frac{0.1f_{cm28}}{6+0.1f_{cm28}}\right)^{2.5}(10^{-6})$	α_{bs} = Defined below. f_{cm28} = Mean concrete compressive strength at 28 days (MPa)
$\beta_{bs}(t)$	$1-\exp(-0.2t^{0.5})$	–
α_{bs}	800 for cement class 32.5 N 700 for cement class 32.5 R and 42.5 N 600 for cement class 42.5 R, 52.5 N, and 52.5 R	–
ε_{cds0}	$((220+110\alpha_{ds1})\exp(-\alpha_{ds2}f_{cm28}))(10^{-6})$	α_{ds1} = Defined below. α_{ds2} = Defined below. f_{cm28} = Mean concrete compressive strength at 28 days (MPa)
α_{ds1}	3 for cement class 32.5 N 4 for cement class 32.5 R and 42.5 N 6 for cement class 42.5 R, 52.5 N, and 52.5 R	–
α_{ds2}	0.13 for cement class 32.5 N 0.12 for cement class 32.5 R, 42.5 N 0.12 for cement class 42.5 R, 52.5 N, 52.5 R	–
β_{RH}(RH)	$-1.55(1-\left(\frac{RH}{100}\right)^3)$ for 40% $\le RH <$ 99% 0.25 for 99% $\le RH$	RH = Relative humidity (%)
$\beta_{ds}(t-t_s)$	$\left(\frac{(t-t_s)}{(t-t_s)+0.035h^2}\right)^{0.5}$	$t-t_s$ = Duration of drying (day) h = Defined below.
β_{s1}	$\left(\frac{35}{f_{cm28}}\right)^{0.1} \le 1$	f_{cm28} = Mean concrete compressive strength at 28 days (MPa)
h	$\frac{2A_c}{(u)}$	A_c = Cross-sectional area u = Perimeter of the member in contact with atmosphere

Creep compliance in the EC2 model is predicted based on the concrete age, time of loading, relative humidity, volume-to-surface ratio, cement type, compressive strength, and temperature. According to this model, the creep coefficient at the concrete age of t (in days) is estimated following Eqs. (33) and (34).

$$\phi(t,t_0) = \phi_0\beta_c(t,t_0) \tag{33}$$

$$\beta_c(t,t_0) = \left[\frac{(t-t_0)}{\beta_H+(t-t_0)}\right]^{0.3} \tag{34}$$

where ϕ_0 is the notional creep coefficient, $\beta_c(t,t_0)$ is a coefficient that accounts for the time development of creep, t_0 is the concrete age at the time of loading (in days), and β_H is to account for relative humidity as defined in Table 10. The EC2 model also allows for

Table 12
Factors and constants for creep compliance in the fib model.

Correction Factor	Equation	Variables
$\beta_{bc}(f_{cm})$	$\frac{1.8}{f_{cm28}^{0.7}}$	f_{cm28} = Mean concrete compressive strength at 28 days (MPa)
$\beta_{bc}(t,t_0)$	$\ln\left(\left(\frac{30}{t_{0,adj}}+0.035\right)^2(t-t_0)+1\right)$	$t_{0,adj}$ = Adjusted age of concrete at loading (day)
$\beta_{dc}(f_{cm})$	$\frac{412}{f_{cm28}^{1.4}}$	f_{cm28} = Mean concrete compressive strength at 28 days (MPa)
$\beta(RH)$	$\frac{1-RH/100}{\sqrt[3]{0.1(\frac{h}{100})}}$	RH = Relative humidity (%) h = Defined below.
h	$\frac{2A_c}{(u)}$	A_c = Cross-sectional area u = Perimeter of the member in contact with atmosphere
$\beta_{dc}(t_0)$	$\frac{1}{(0.1+t_{0,adj}^{0.2})}$	$t_{0,adj}$ = Adjusted age of concrete at loading (day)
$\beta_{dc}(t,t_0)$	$\left(\frac{(t-t_0)}{\beta_H+t-t_0}\right)^{\gamma(t_0)}$	$\gamma(t_0)$ = Defined below. β_H = Defined below.
$\gamma(t_0)$	$\frac{1}{(2.3+\frac{3.5}{\sqrt{t_{0,adj}}})}$	$t_{0,adj}$ = Adjusted age of concrete at loading (day)
β_H	$1.5h+250\alpha_{f_{cm}} \le 1500\alpha_{f_{cm}}$	$\alpha_{f_{cm}}$ = Defined below.
$\alpha_{f_{cm}}$	$\left(\frac{35}{f_{cm28}}\right)^{0.5}$	f_{cm28} = Mean concrete compressive strength at 28 days (MPa)

modifications to account for unusual temperature ranges.

2.6. fib model

In the fib model, a set of equations are presented to determine drying shrinkage strain and creep coefficient as a function of time [40]. Shrinkage strain in this model is predicted based on the concrete age, time of drying, relative humidity, volume-to-surface ratio, cement type, compressive strength, and temperature. Shrinkage strain according to the fib model is defined following Eq. (35).

$$\varepsilon_{cs}(t,t_s) = \varepsilon_{cds}(t,t_s) + \varepsilon_{cbs}(t) \tag{35}$$

where $\varepsilon_{cs}(t,t_s)$ is the total shrinkage at the concrete age of t (in days), t_s is the concrete age at the beginning of drying (in days), $\varepsilon_{cds}(t,t_s)$ is the drying shrinkage component, and $\varepsilon_{cbs}(t)$ is the basic shrinkage component. The drying component of shrinkage is defined according to Eqs. (36) and (37).

$$\varepsilon_{cds}(t,t_s) = \varepsilon_{cds,0}(f_{cm28})\beta_{RH}(RH)\beta_{ds}(t-t_s) \tag{36}$$

$$\beta_{ds}(t-t_s) = \left(\frac{(t-t_s)}{(t-t_s)+0.035h^2}\right)^{0.5} \tag{37}$$

where $\varepsilon_{cds,0}(f_{cm28})$ is the notional drying shrinkage coefficient, $\beta_{RH}(RH)$ is the coefficient of ambient relative humidity defined in Table 11, $\beta_{ds}(t-t_s)$ is the time development factor for drying shrinkage, and h is the notional member size defined in Table 11.

The basic component of shrinkage is defined according to Eqs. (38) and (39).

$$\varepsilon_{cbs}(t) = \varepsilon_{cbs,0}(f_{cm28})\beta_{bs}(t) \tag{38}$$

$$\beta_{bs}(t) = 1 - e^{\left[-0.2(t)^{0.5}\right]} \tag{39}$$

where $\varepsilon_{cbs,0}(f_{cm})$ is the notional basic shrinkage coefficient defined in Table 11, and $\beta_{bs}(t)$ is the time development factor for basic shrinkage.

Creep compliance in the fib model is predicted based on the concrete age, time of loading, relative humidity, volume-to-surface ratio, cement type, compressive strength, and temperature. The creep coefficient at the concrete age of t (in days) is determined according to Eq. (40).

$$\phi(t,t_0) = \phi_{dc}(t,t_0) + \phi_{bc}(t,t_0) \tag{40}$$

where $\phi(t,t_0)$ is the total creep coefficient at the concrete age of t (in days), t_0 is the concrete age at the beginning of drying (in days), $\phi_{dc}(t,t_0)$ is the drying creep coefficient, and $\phi_{bc}(t,t_0)$ is the basic creep coefficient. The drying and basic components of the creep coefficient are defined according to Eqs. (41) and (42), respectively.

Table 13
Overview of the input parameters used in various shrinkage and creep prediction models.

Input	AASHTO	ACI	B3	CEB	EC2	fib
Age at the start of drying	•	•	•	•	•	•
Age at the start of loading	•	•	•	•	•	•
Curing method	•	•	•		•	•
Relative humidity	•	•	•	•	•	•
Volume-to-surface ratio	•	•	•	•	•	•
Water content			•			
Slump		•				
28-day mean compressive strength	•		•	•	•	•
Fine aggregate ratio		•				
Total aggregate content			•			
Cement type		•	•	•	•	•
Cement content		•	•			
Temperature				•	•	•
Air content		•				
28-day modulus of elasticity			•	•		
Specimen shape			•			

$$\phi_{dc}(t,t_0) = \beta_{dc}(f_{cm})\beta(RH)\beta_{dc}(t_0)\beta_{dc}(t,t_0) \tag{41}$$

$$\phi_{bc}(t,t_0) = \beta_{bc}(f_{cm})\beta_{bc}(t,t_0) \tag{42}$$

The coefficients of compressive strength, $\beta_{dc}(f_{cm})$ and $\beta_{bc}(f_{cm})$, relative humidity, $\beta(RH)$, and time development, $\beta_{dc}(t,t_0)$ and $\beta_{bc}(t,t_0)$, are listed in Table 12. Similar to the B3, CEB and EC2 models, the fib model differentiates between basic and drying creeps. The fib model also allows for modifications to account for unusual temperature ranges.

3. Comparison of model variables

3.1. Model Inputs

A summary of the input parameters required for each of the presented models is provided in Table 13. The age of concrete at the start of drying and loading, relative humidity, and specimen volume-to-surface ratio are the common input parameters directly considered by the six models investigated in the current study. Moreover, all models, except the CEB model, take the curing method into account. Despite overall similarities, there are also differences between the input parameters of these models. Specifically, the models start to differ in their accounting of the water contained in the concrete mixture. The amount of water affects the fresh state properties, microstructural porosity, hardened state performance, and thus, the time-dependent behavior of the concrete. The B3 model is the only model that directly receives the water content as an input. In fact, water content, slump, and strength are all related. Hence, all the models, except ACI 209, account for water content through the 28-day mean compressive strength of the concrete. The ACI 209 model, however, considers water content by taking the slump value as input.

The aggregate properties (e.g., type, shape, size, and content) are known to affect the concrete's shrinkage and creep behavior through various mechanisms, such as restraining volumetric change, causing excessive water absorption, while changing the mixture's elasticity and stiffness. Among the six models investigated in the current study, only two models directly consider aggregate content and size as inputs. The fine aggregate ratio and total aggregate content are the inputs specifically taken into consideration in the ACI 209 and B3 models, respectively. Focusing on binders, the properties of cement, including particle size distribution, setting time, and strength, play a pivotal role in the concrete's time-dependent properties. Except for the AASHTO model, all models directly take the type of cement into account, among which ACI 209 and B3 models consider the cement content as well. In addition to relative humidity, the temperature is an environmental stressor, mostly impacting the drying shrinkage behavior. The temperature effect is taken as input by the CEB, EC2, and fib models. The modulus of elasticity and specimen shape are specific inputs only considered in the B3 model. The ACI 209 model is the only model that takes into consideration the impact of air content.

Reviewing the number of inputs required for each model sheds light on the overall complexity and possible flexibility of that model. Among the six models investigated, the AASHTO model is the simplest model, requiring only six input parameters to predict both shrinkage and creep. The only input for the AASHTO model that represents the concrete mixture is the 28-day mean compressive strength. The CEB, EC2, and fib models require 8 inputs, among which only three inputs of 28-day mean compressive strength, cement type, and 28-day modulus of elasticity are linked to the concrete mixture. This still makes them seemingly simple models. The ACI 209 model utilizes 10 inputs to predict shrinkage and creep. This model includes 5 inputs related to the concrete mixture, i.e., slump, fine aggregate ratio, cement type, cement content, and air content. Lastly, the B3 model requires the most inputs, i.e., 12 inputs, including 6 inputs related to the concrete mixture, i.e., water content, 28-day mean compressive strength, total aggregate content, cement type, cement content, and 28-day mean modulus of elasticity. Concerning the number and variety of inputs that each model requires, it can be inferred that the ACI 209 and B3 models are the most robust models among the models considered.

3.2. Model outputs

The outputs of all the models are similar, as they all calculate shrinkage strain and creep compliance or creep coefficient as a function of time. Since creep compliance and creep coefficient are related, this does not constitute a significant difference between the models. The models also share some notable limitations with respect to their outputs. First, they predict a mean value for shrinkage strain. The drawback to this approach is disregarding the fact that shrinkage varies throughout the cross-section of a concrete member. This means that internal strains caused by differential shrinkage are not accounted for in the models. Another limitation shared by all the models is that their creep predictions are valid for relatively low stress levels, i.e., around 40% or less of the concrete compressive strength at the time of loading. Furthermore, the models predict creep only under a constant sustained load. Loads that vary with time are not captured by the discussed models.

In addition to predicting shrinkage and creep as a function of time, all the models, except for the AASTHO model, provide ultimate values of shrinkage and creep. Regarding shrinkage, only the CEB, EC2, and fib models break down the calculation of shrinkage into autogenous and drying shrinkage. For creep, only the B3 and fib models break down the calculation of creep into two components of basic creep and drying creep. Since all the models share certain limitations that can influence the accuracy of the predictions, the use of data-enabled prediction strategies is recommended. Such models take into consideration a range of inputs, especially those associated with mixture properties, and build on a set of testing and training to determine the variables that contribute the most. It should be noted that the current study covered investigations and side-by-side comparisons of six shrinkage and creep prediction models primarily utilized in the United States and Europe. There are, however, other capable prediction models available. Among them are the B4 model [43], GL2000 model [44], and JSCE model [45]. While the referenced models were not included in this study, they are worthy of consideration for the prediction of shrinkage and creep effects.

4. Data selection and model calibration

There is an abundance of shrinkage and creep experiments that have been performed and published to date. Among them, this study utilized experimental test data from the NU-ITI database [41,42] to calibrate and analyze the introduced six models. This database, formerly known as the RILEM database, was established 40 years ago and currently hosts a suite of data from shrinkage and creep tests. Over its life, this database has been expanded in collaboration with the ACI, CEB, and RILEM and is now maintained by the Northwestern University Infrastructure Technology Institute. The expanded database hosts data for (approximately) 490 shrinkage tests and 620 creep tests, along with their supporting references [41,42]. The primary purpose of the referenced database is to evaluate prediction models, making it suitable for calibrating and comparing the models explored in the current study. Given the wealth of data available in the NU-ITI database, a set of selection criteria must be employed. For concrete mixtures, the current study focused on Class A concrete specified by AASHTO [36]. This concrete class was a suitable choice, as it is commonly used for a wide range of structural elements (with only a few exceptions, e.g., for concrete directly exposed to saltwater). Hence, this class is deemed as the most inclusive class of concrete, which can be made with any conventional cement (regardless of the source/origin). For curing, the datasets were selected from the concrete specimens that had been subjected to moist curing for at least two full days. For relative humidity, the selected experiments had been performed at a relative humidity of 50%− 80% and at a constant temperature of around 20 degrees of Celsius.

A number of shrinkage and creep experiments were evaluated to ensure meeting the selection criteria, while providing appropriate statistical representations. The shrinkage models were investigated for unrestrained shrinkage by utilizing available experimental test data from the NU-ITI database. Ten experiments from the NU-ITI database were selected to calibrate the shrinkage models with experimental conditions presented in Table A.1. The average 28-day compressive strength of all selected specimens for shrinkage calibration and analysis was 4.88 ksi (33.7 MPa). The concrete's average age at the start of drying was 6.2 days. Additionally, all selected shrinkage experiments had been performed at a relative humidity of 65%. The creep models were also assessed for compressive creep by utilizing available experimental test data from the NU-ITI database. Twenty experiments from the NU-ITI database were selected to calibrate the creep models. The properties of each experiment selected are presented in Table A.2. The selected specimens for creep calibration and comparison had an average 28-day compressive strength of 4.86 ksi (33.5 MPa). The average age of the concrete at the start of loading was 22.6 days. The selected creep experiments had an average relative humidity of 57%. As the NU-ITI database does not report the concrete slump, which is needed for the ACI 209 model, a uniform slump of 3.5 in. (8.9 cm) was assumed for all the experiments considered.

The performance of each shrinkage and creep model was first investigated with no model calibration. Then, to further refine the outputs, a calibration approach was employed such that each model was calibrated to the data obtained from the NU-ITI database. This approach introduced 2 calibration factors for each model. Among the six models, only the ACI 209 model provided direct guidance for this type of calibration. To determine the calibration factors for shrinkage and creep models, the calibration process was performed to first adjust the long-term shrinkage/creep behavior and then the rate of shrinkage/creep development over time. For this purpose, a single factor was first applied to the ultimate value of shrinkage/creep strain in each model. This factor was adjusted for each model to best match the model to the experiments. For example, if a model was found to predominantly underestimate the shrinkage recorded in the experiments, this factor was set to a value higher than unity to improve the model. A second factor was then applied to the time development component of each model. This second factor modified the shape of the shrinkage/creep curve for each model. As an example, if the long-term predicted shrinkage/creep of a model closely matched that of the experiments but the rate of shrinkage/creep development differed notably, this factor was set to values different than unity to alter the rate at which shrinkage/creep development was predicted. The ACI 209 model had two well-defined, built-in coefficients that serve as this second factor. Similarly, in the EC2

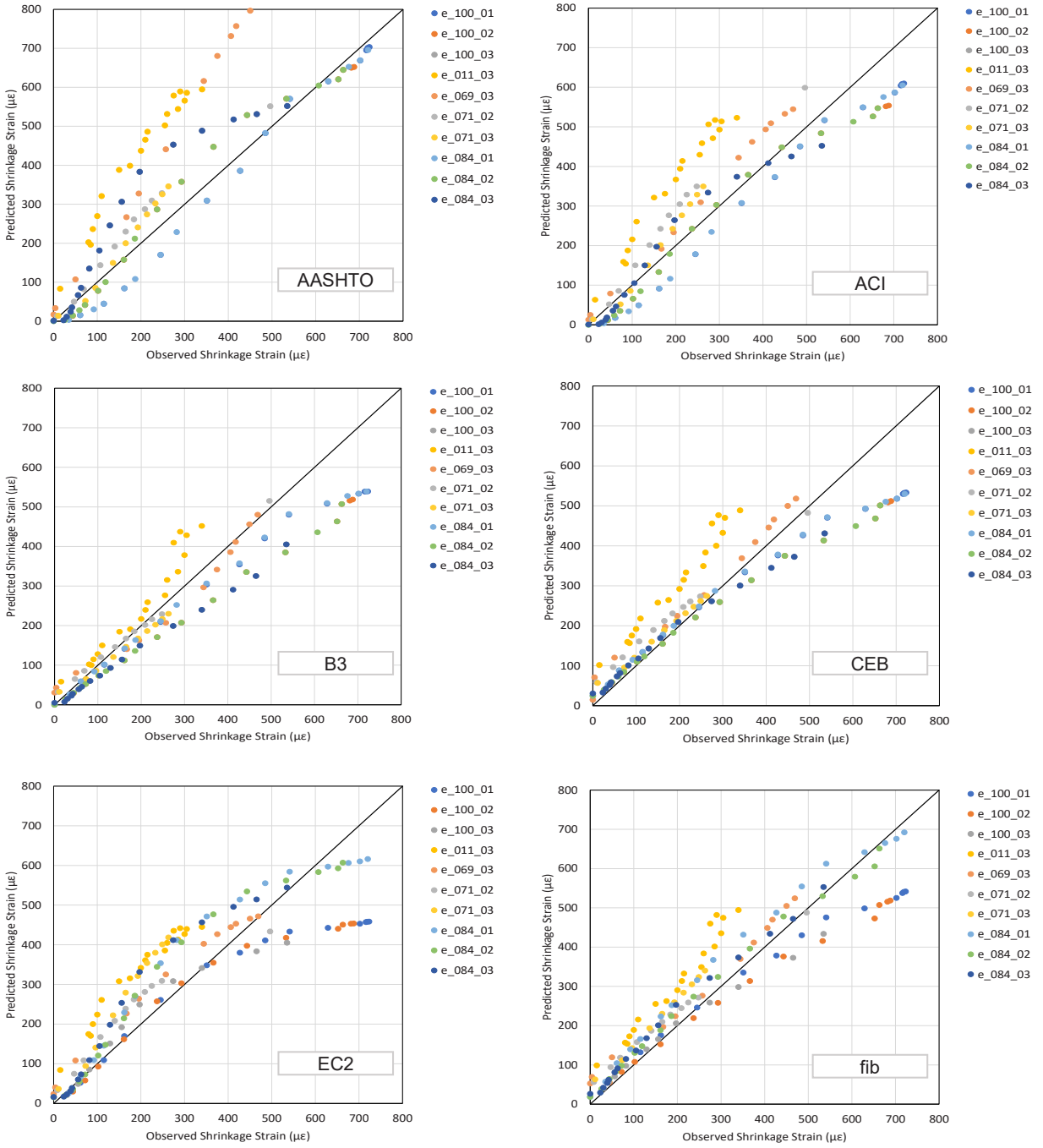

Fig. 1. Performance of the six uncalibrated shrinkage models.

model, a calibration procedure was allowed, in which a parameter for the amplitude and a parameter for the kinetics can be adjusted for each component of shrinkage and creep. In this study, Eq. (43) was utilized as the main expression for the calibration process:

$$Y = UX\beta(t - t_0)^T \tag{43}$$

where Y is the calibrated value, X is the original value predicted by the model (uncalibrated), U is the ultimate calibration factor, β is the time development function included in each model, and T is the time development calibration factor. The required factors were calibrated such that each model had only one value for each factor that covered every experiment. Those values were obtained through an iterative approach to achieve the best match between the models and recorded test data. The following section provides the calibration factors and the prediction performance of the introduced shrinkage and creep models.

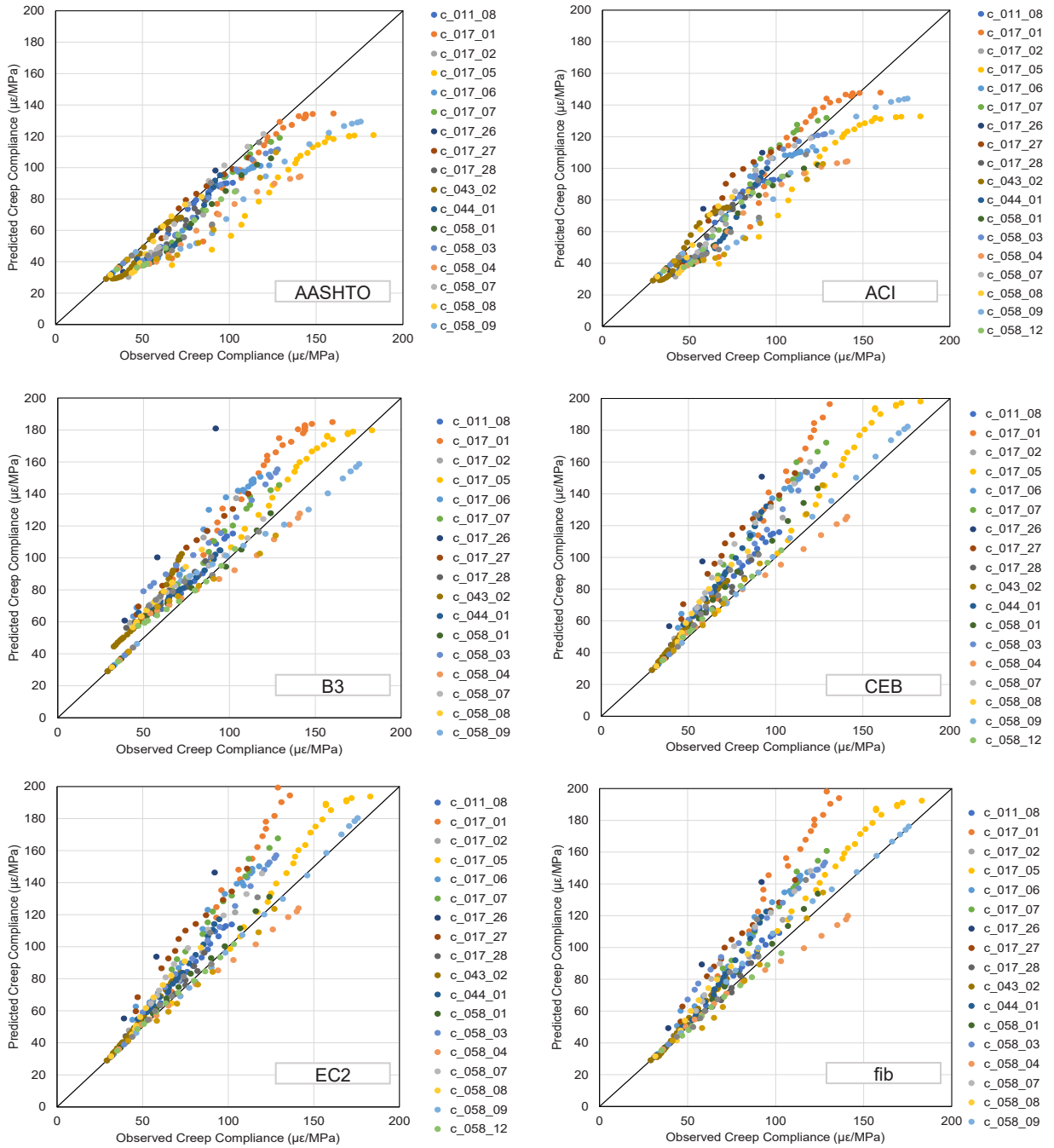

Fig. 2. Performance of the six uncalibrated creep models.

Table 14
Performance of the uncalibrated shrinkage prediction models.

		AASHTO	ACI	B3	CEB	EC2	fib
Coefficient of determination (R^2)		0.72	0.81	0.77	0.66	0.69	0.83
Residuals	Overestimate (%)	62.14	49.29	24.29	66.43	70.00	77.86
	Underestimate (%)	37.86	50.71	75.71	33.57	30.00	22.14

Table 15
Performance of the uncalibrated creep prediction models.

		AASHTO	ACI	B3	CEB	EC2	fib
Coefficient of determination (R^2)		0.61	0.84	0.75	0.71	0.78	0.78
Residuals	Overestimate (%)	7.85	35.15	83.96	88.40	82.25	79.52
	Underestimate (%)	92.15	64.85	16.04	11.60	17.75	20.48

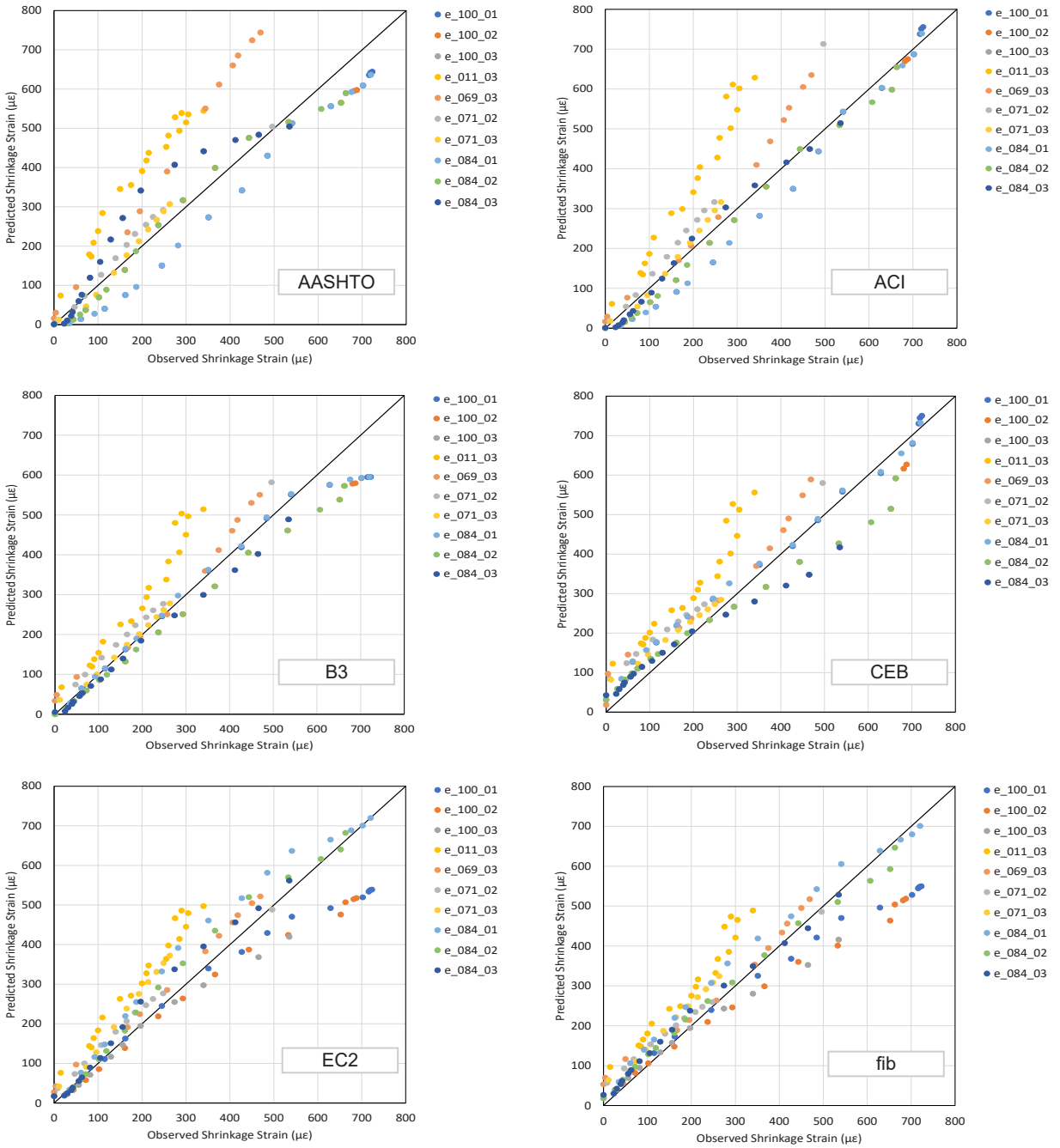

Fig. 3. Performance of the six calibrated shrinkage models.

Table 16
Calibration factors and performance of the calibrated shrinkage prediction models.

		AASHTO	ACI	B3	CEB	EC2	fib
Coefficient of determination (R^2)		0.77	0.86	0.89	0.83	0.84	0.84
Residuals	Overestimate (%)	56.40	47.90	48.57	76.43	65.71	74.29
	Underestimate (%)	43.60	52.10	51.43	23.57	34.29	25.71
Calibration factor (U_{sh})		0.92	1.31	1.10	1.53	1.20	1.02
Calibration factor (T_{sh})		0.98	0.83	1.05	0.75	0.81	0.95

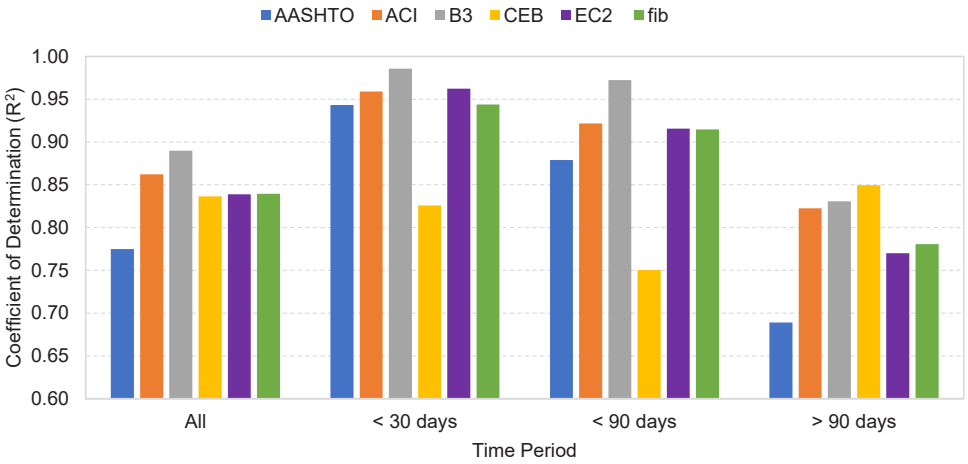

Fig. 4. Comparison of the coefficient of determination (R^2) of the calibrated shrinkage prediction models in different time periods.

Table 17
Residuals of the calibrated shrinkage prediction models.

	Stage		AASHTO	ACI	B3	CEB	EC2	fib
Residuals	< 30 days	Overestimate (%)	45.00	33.33	53.33	100.00	68.33	96.67
		Underestimate (%)	55.00	66.67	46.67	0.00	31.67	3.33
	> 90 days	Overestimate (%)	56.36	58.18	40.00	50.91	58.18	45.45
		Underestimate (%)	43.64	41.82	60.00	49.09	41.82	54.55

5. Results and discussion

5.1. Original uncalibrated models

For each of the six models, data from the selected experiments were plotted against the predicted values of the original uncalibrated models. A graphical comparison of the uncalibrated shrinkage and creep models to data from the NU-ITI database is presented in Figs. 1 and 2, respectively. A predicted data point perfectly matches the experimental value if it lands on the line with a slope of one beginning from the origin. Residuals were calculated for each point by subtracting the experimentally measured shrinkage values from the predicted values. When the residual value is positive, the model is overestimating, and when it is negative, the model is underestimating. The coefficient of determination (R^2) was also used to measure the performance of the models by quantifying the correlation between the predicted and recorded values for each model. Tables 14 and 15 present the R^2 values and residuals in each of the six shrinkage and creep models, respectively. Considering the overall performance of the uncalibrated models in shrinkage and creep prediction, the ACI 209 model outperformed other models with the R^2 values of 0.81 and 0.84 for the shrinkage and creep models, respectively. This superior performance can be attributed to the large variety and number of parameters (10 inputs), as well as the built-in tuning time-ratio constant included in the ACI 209 model.

5.2. Calibrated shrinkage models

Following the approach described in Section 4, each of the six models was calibrated and their performance was studied. A graphical comparison of the calibrated models (i.e., models with a single value for each calibration factor) to data from the NU-ITI database is presented in Fig. 3. Table 16 presents the R^2 values, residuals, and calibration factors for the ultimate shrinkage strain (U_{sh}) and time development (T_{sh}) in each of the six model. Overall, The B3 and ACI 209 models were found to perform the best of all the

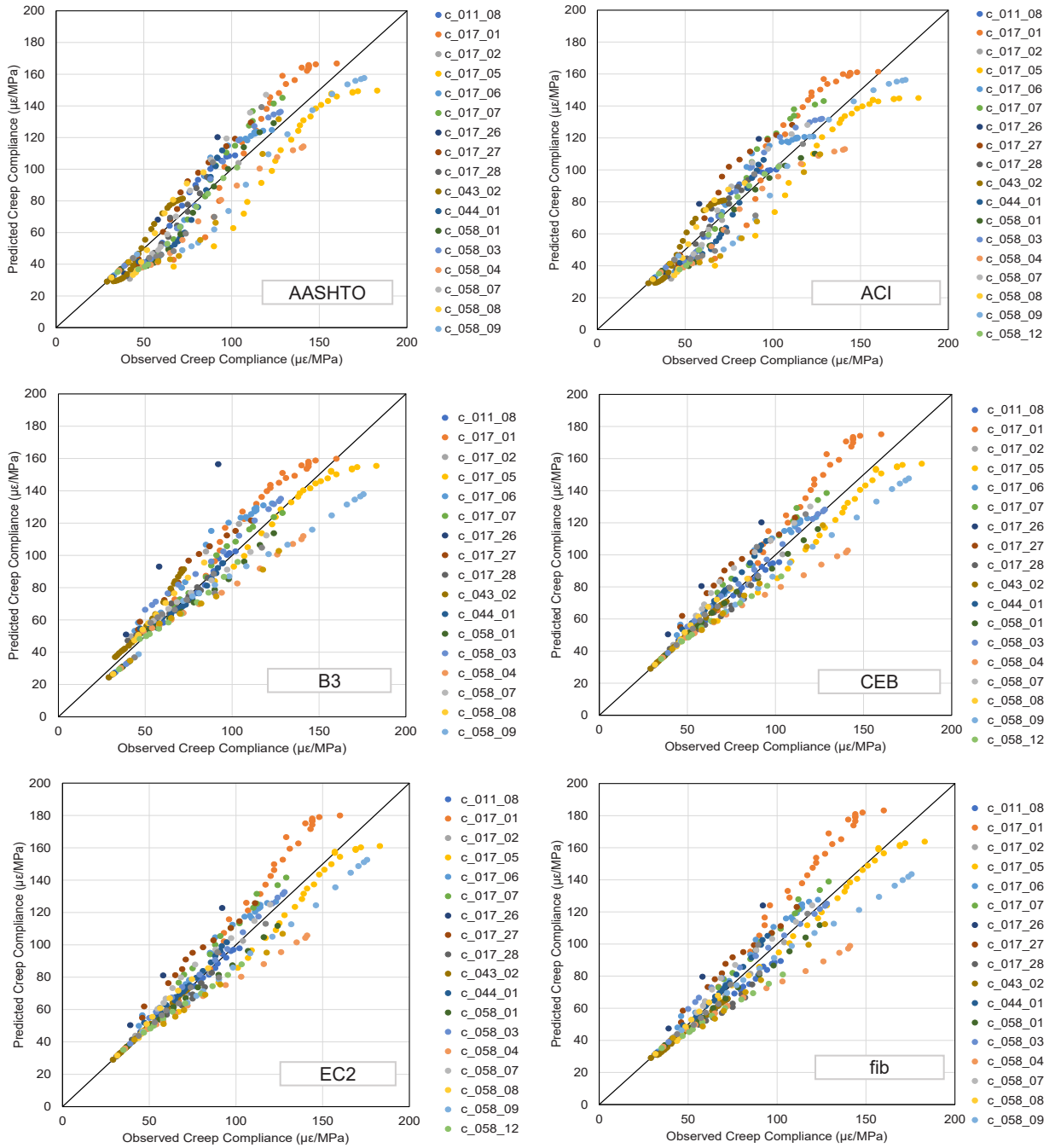

Fig. 5. Performance of the six calibrated creep models.

Table 18
Calibration factors and performance of the calibrated creep prediction models.

		AASHTO	ACI	B3	CEB	EC2	fib
Coefficient of determination (R^2)		0.87	0.88	0.87	0.89	0.89	0.88
Residuals	Overestimate (%)	39.25	46.42	54.95	53.92	52.22	43.00
	Underestimate (%)	60.75	53.58	45.05	46.08	47.78	57.00
Calibration factor (U_{cr})		1.34	1.13	0.84	0.75	0.79	0.53
Calibration factor (T_{cr})		0.99	0.99	1.11	0.99	1.01	0.97

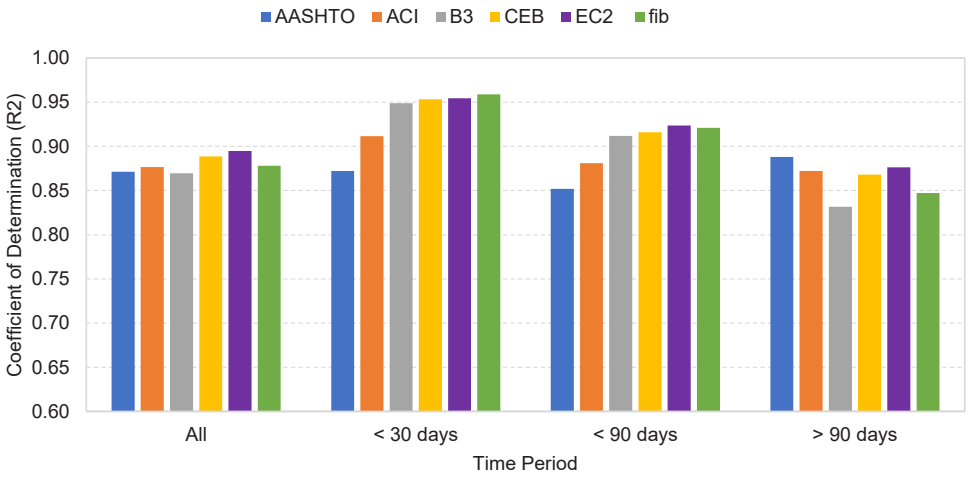

Fig. 6. Comparison of the coefficient of determination (R^2) of the calibrated creep prediction models in different time periods.

Table 19
Residuals of the calibrated creep prediction models.

	Stage		AASHTO	ACI	B3	CEB	EC2	fib
Residuals	< 30 days	Overestimate (%)	5.67	19.15	53.19	53.90	47.52	41.13
		Underestimate (%)	94.33	80.85	46.81	46.10	52.48	58.87
	> 90 days	Overestimate (%)	72.48	66.97	58.72	53.21	56.88	42.20
		Underestimate (%)	27.52	33.03	41.28	46.79	43.12	57.80

shrinkage models with the R^2 values of 0.89 and 0.86, respectively. This can be supported by the fact that these two models incorporate more parameters related to the concrete mixture, resulting in higher accuracy. On the other hand, the AAHTHO model had the lowest prediction accuracy with the R^2 value equal to 0.77. Previous studies showed similar findings/trends for the original uncalibrated form of these prediction models. Therefore, it can be inferred that even the calibration of shrinkage rate and ultimate values cannot completely compensate for the shortage of model inputs, revealing the pivotal role of relevant input parameters in selecting appropriate models. Considering the residuals calculated for each model, it can be noted that the AASHTO, CEB, EC2, and fib models tend to overestimate the shrinkage strain values. The ACI 209 and B3 models, however, exhibited a more balanced distribution between the positive and negative residuals and were considered the best performing models.

Additionally, R^2 and residual values were calculated over a set of time periods for each model. This allowed insights into how the models behave during just the early-age period or the long-term period of shrinkage. The early-age period considered was the first 30 days of a specimen being exposed to drying and the long-term period considered was any time after the first 90 days of being exposed to drying. As shown in Fig. 4, during the early-age and long-term periods, the B3 and ACI 209 models outperformed other models. This observation was consistent with their overall performance over the entire time. For the early-age period, which is crucial to shrinkage sensitive structures, all models except the CEB model, performed comparable to the B3 model with an average R^2 value of 0.95, compared to the R^2 value of 0.99 in the B3 model. Although the result obtained from the CEB model demonstrated a high R^2 and balanced distribution between the positive and negative residuals in long term (> 90 days), it was observed that this model tends to overestimate the shrinkage strain in the first 30 days (as reflected in Table 17), resulting in the lowest R^2 at the early-age period. This can be associated with the fact that the CEB model predicted a higher shrinkage rate in the early stage than actual values. The lowest calibration factor for the rate of shrinkage (T_{sh}) corresponded to the CEB model (Table 16), justifying the need for applying a lower shrinkage rate to this model. As presented in Table 17, the fib model mostly overestimated the shrinkage strain values in early stage (< 30 days). Overall, after the first 90 days of being exposed to drying, all the six models showed a more balanced distribution between the positive and negative residuals compared to that of the first 30 days.

5.3. Calibrated creep models

Similar to shrinkage-related investigations, data from the selected creep experiments were plotted against the predicted values of the calibrated models (i.e., models with a single value for each calibration factor). A graphical comparison of the calibrated models to data from the NU-ITI database is presented in Fig. 5. As with the shrinkage model analysis, the R^2 value was used to measure the performance of the models by quantifying the correlation between the predicted values and recorded values for each model. Residuals were also calculated for each point by subtracting the experimentally measured creep values from the predicted values. Table 18 presents the R^2 values, residuals, and calibration factors for the ultimate creep strain (U_{cr}) and time development (T_{cr}) in each of the six model. Overall, the performance of all calibrated creep prediction models was similar, having the R^2 value in the range of 0.87–0.89.

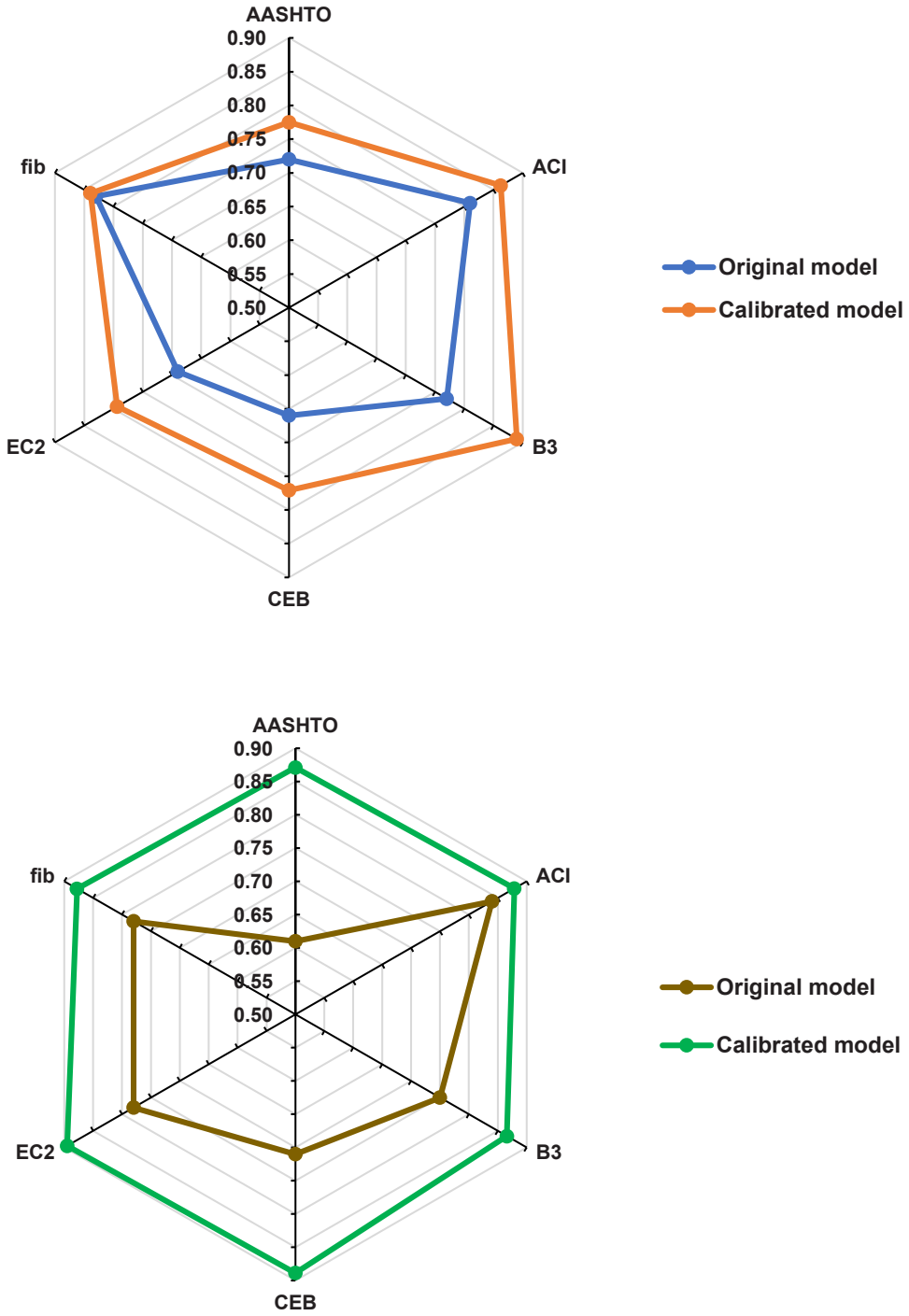

Fig. 7. Comparison of the performance between the original (uncalibrated) and the calibrated shrinkage prediction models.

The calibration factors that influenced time development (T_{cr}) were found to barely differ from unity among the models. All calibrated models, except the AASHTO model, indicated almost a balanced distribution between the positive and negative residuals. Thus, it can be inferred that the calibrated creep prediction models provided higher accuracy and less dispersion compared to the shrinkage prediction models.

R^2 and residual values were also calculated over various time periods for each model. The R^2 values for each creep model are presented in Fig. 6. Despite having similar overall R^2, creep predictive models show different performances in the early-age and long-term periods. The ACI 209 and AASHTO models exhibited almost the same accuracy at both early age and long term (R^2 between 0.85

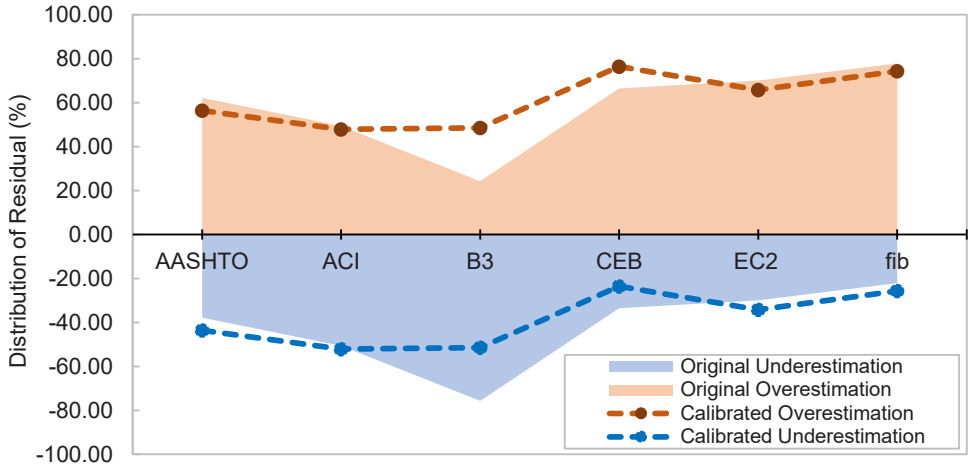

Fig. 8. Distribution of residuals for the original and calibrated shrinkage prediction models. Positive and negative values represent the percentage of overestimated and underestimated shrinkage effects, respectively.

and 0.89). However, over the early-age period, the AASHTO and ACI 209 models had a notably lower R^2 values of 0.87 and 0.91, respectively, compared to the other models with the average R^2 values approaching 0.95. It is important to note that the ACI 209 shrinkage model relies on slump as its only input regarding the concrete water content, making it the only model considered in this study that does not utilize the 28-day mean compressive strength to account for water content. Since this factor affects the magnitude and rate of shrinkage and creep, the constant slump of 3.5 in. (8.9 cm) assumed in the current study required the ACI 209 model to utilize the same water content for all the experiments, while the other models were able to consider the actual water contents recorded for each experiment. However, even with this situation, the ACI 209 shrinkage model compared reasonably well with the other models.

Apart from these two models, other models showed higher accuracy during the early-age period (i.e., first 30 days), achieving R^2 values above 0.94. However, during the long-term period, they showed lower R^2 values compared to the early stage and overall performance. This can be associated with the fact that the early-stage creep strains are mainly affected by the creep rate, and all the studied creep models exhibited a close correlation with experimental creep rate values and did not require significant calibration. This is reflected in the T_{cr} calibration factors, which were found to be close to one (Table 18). However, these creep models struggle with an accurate prediction of ultimate creep strain, which, in turn, adversely affects their long-term performance, despite the calibration factors introduced. As presented in Table 19, all calibrated models, except the AASHTO and ACI 209 models, provided an almost balanced distribution between the positive and negative residuals in both early-age and long-term stages. The AASHTO and ACI 209 models, however, mostly underestimated the creep strain values in the early stage ($<$ 30 days).

5.4. Improvements introduced by calibration factors

Using the same database, the performance of the models calibrated in this study was compared to their original uncalibrated forms. Fig. 7 shows that the calibration approach used in this study enhanced the performance of the shrinkage prediction models and increased their R^2 values. Specifically, the improvement was highest for the CEB model, increasing its R^2 from 0.66 to 0.84 (i.e., 27% growth). On average, the R^2 value improved by 13% upon calibrating the shrinkage rate and its ultimate value. Comparing the original and calibrated models, the distribution of residuals was also evaluated, as shown in Fig. 8. It can be noted that the employed calibration approach decreased the tendency of all the models, except the CEB model, to either overestimate or underestimate the shrinkage strain values.

Fig. 9 shows the impact of calibration on the creep prediction models. Similar to the trend observed in the shrinkage prediction models, the calibration approach improved the performance of the creep prediction models and increased their R^2 values. Specifically, it had the highest positive impact on the performance of the AASHTO model, increasing its R^2 from 0.61 to 0.87 (i.e., 43% growth). On average, the R^2 value increased by 19% upon calibrating the creep rate and its ultimate value. It must be highlighted that, although original creep models showed various performance levels with a broad range of R^2 values (i.e., from 0.61 to 0.84), their calibrated forms exhibited almost similar accuracy. The original and calibrated models were also compared in terms of the distribution of residuals, as shown in Fig. 10. It can be observed that the employed calibration approach successfully decreased the tendency of all the models to either overestimate or underestimate the creep strain values. The calibrated creep models almost showed a balanced distribution between the positive and negative residuals.

6. Conclusions

A set of shrinkage and creep models were systematically examined to determine their prediction capabilities and limitations. The investigated models included some of the most commonly used models, including AASHTO, ACI 209, B3, CEB, EC2, and fib models. All

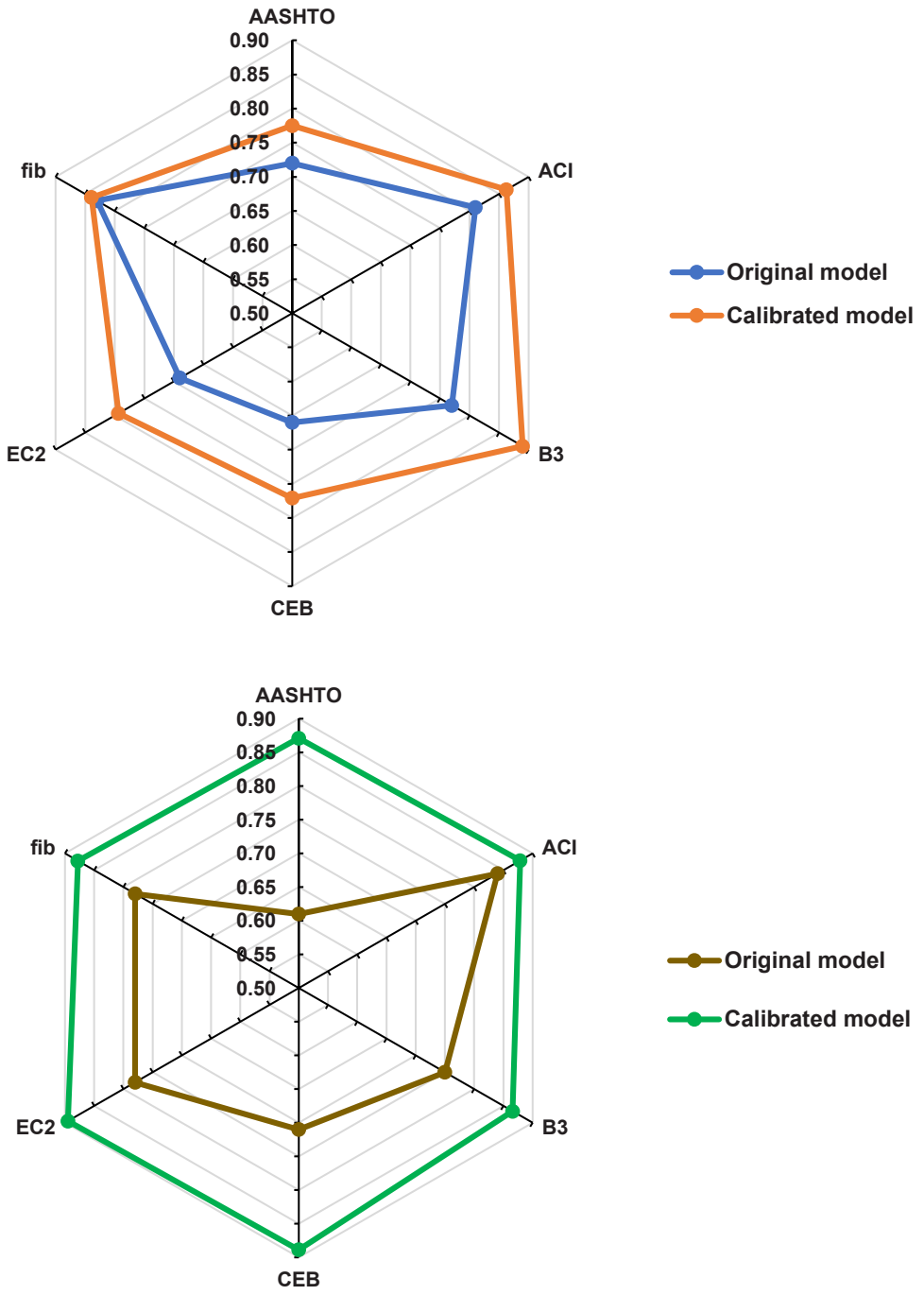

Fig. 9. Comparison between the performance of the original (uncalibrated) and the calibrated creep prediction models.

these models share the same fundamental basis. Thus, the preference for using a specific model heavily relies on its accuracy and simplicity (especially if only limited input parameters are known/available). In the absence of any similar holistic study in the literature, the performance of each model was quantified in the current study by comparing the model outputs to the experimental test data from the NU-ITI shrinkage and creep database. Calibration factors were then introduced for each model to improve their performance. Based on this investigation, the following conclusions were drawn:

- Considering the overall performance of the uncalibrated models in shrinkage and creep prediction, the ACI 209 model was found to outperform the other five models. This performance can be attributed to the large variety and number of parameters (10 inputs), as well as the built-in tuning time-ratio constant included in the ACI 209 model.

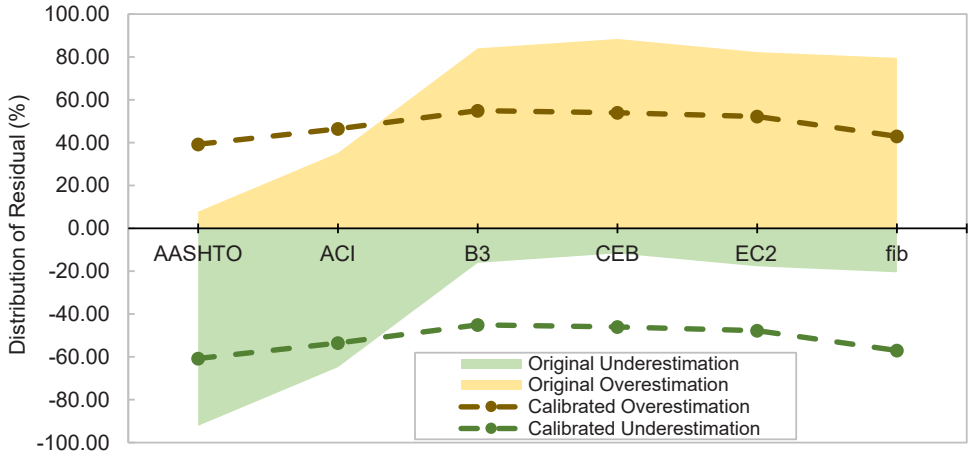

Fig. 10. Distribution of residuals for the original and calibrated creep prediction models. Positive and negative values represent the percentage of overestimated and underestimated creep effects, respectively.

- The calibrated B3 and ACI 209 models were generally identified as the most performant models with the R^2 values of 0.89 and 0.86, respectively. Furthermore, they exhibited a balanced distribution between the positive and negative residuals (overestimated and underestimated values). However, for the early-age period, which is crucial to shrinkage sensitive structures, all the other calibrated models, except the CEB model, performed similar to the B3 model with the average R^2 value of 0.95, compared to the R^2 value of 0.99 obtained for the B3 model.
- Concerning creep, the investigated calibrated models provided the R^2 values in the range of 0.87–0.89, with no model lagging significantly behind the others. The calibration factors that influence time development were found to barely differ from unity among the models. All calibrated models, except the AASHTO model, indicated an almost balanced distribution between the positive and negative residuals. Overall, it can be inferred that the calibrated creep prediction models offer higher accuracy and less dispersion compared to the shrinkage prediction models.
- The calibration approach used in this study enhanced the performance of the shrinkage and creep prediction models by increasing their accuracy and decreasing their tendency to either overestimate or underestimate strain values. On average, the R^2 values increased by 13% and 19% upon calibrating the studied shrinkage and creep prediction models, respectively.
- Another factor to consider when selecting shrinkage and creep models is the simplicity of the models. Comparing the top two performant models, i.e., ACI 209 and B3, the former was clearly the simpler model. While maintaining the second-highest number of inputs, the ACI 209 model required fewer steps and simpler calculations compared to the B3 model, which had the highest number of inputs. In this regard, the ACI 209 model was found to be a well-suited model for the purpose of shrinkage and creep analyses in practical applications.

With a side-by-side review and comparison of various shrinkage and creep models, the outcome of this study offers fundamental and practical insights to properly select and utilize shrinkage and creep models, taking into consideration their key contributing factors for maximum accuracy.

Declaration of Competing Interest

The authors declare that they have no known competing financial interests or personal relationships that could have appeared to influence the work reported in this paper.

Data Availability

Data will be made available on request.

Acknowledgments

The support of the Iowa Department of Transportation and Iowa Highway Research Board is gratefully acknowledged. The contents of this manuscript reflect the opinions of the authors and do not necessarily express the views of the sponsoring agencies.

Appendix

Table A.1
Experiments selected from the NU-ITI to calibrate and compare the shrinkage models (w/c is the water-to-cement ratio, a/c is the aggregate-to-cement ratio, and VS is the volume-to-surface ratio).

Database	w/c	a/c	Cement (kg/m^3)	f_{cm28} (MPa)	2VS (mm)	t_0 (day)	Humidity (%)
e_100_01	0.48	5.429	350	33.2	42	7	65
e_100_02	0.48	5.429	350	33.2	80	7	65
e_100_03	0.48	5.429	350	33.2	150	7	65
e_011_03	0.45	5.392	345	35.3	100	7	65
e_069_03	0.45	5.405	353	23.9	75	7	65
e_071_02	0.50	-	350	40.7	75	3	65
e_071_03	0.50	-	350	37.5	75	3	65
e_084_01	0.48	5.428	350	33.2	41.5	7	65
e_084_02	0.48	5.428	350	33.2	80	7	65
e_084_03	0.48	5.428	350	33.2	150	7	65

Table A.2
Experiments selected from the NU-ITI database to calibrate and compare the creep models (w/c is the water-to-cement ratio, a/c is the aggregate-to-cement ratio, and VS is the volume-to-surface ratio).

Database	w/c	a/c	Cement (kg/m^3)	f_{cm28} (MPa)	2VS (mm)	t_0 (day)	Humidity (%)	Stress (MPa)
c_011_08	0.45	5.392	345	35.3	100	28	65	14.22
c_017_01	0.49	4.814	350	33.9	35	7	50	4.91
c_017_02	0.49	4.814	350	33.9	35	21	50	4.91
c_017_05	0.49	4.814	350	33.9	35	7	50	9.81
c_017_06	0.49	4.814	350	33.9	35	21	50	9.81
c_017_07	0.49	4.814	350	33.9	35	28	50	9.81
c_017_26	0.49	4.814	350	33.9	35	28	35	9.81
c_017_27	0.49	4.814	350	33.9	35	28	50	9.81
c_017_28	0.49	4.814	350	33.9	35	28	75	9.81
c_043_02	0.41	5.587	332	40.9	100	28	65	9.40
c_044_01	0.40	5.595	343	27.9	75	28	50	8.83
c_058_01	0.50	6.300	300	29.2	75	28	60	14.71
c_058_03	0.44	5.266	360	37.8	75	7	60	17.66
c_058_04	0.47	5.232	375	39.0	75	17	60	17.66
c_058_07	0.50	6.300	300	29.2	75	28	60	14.71
c_058_08	0.50	5.314	350	33.6	75	28	60	9.81
c_058_09	0.47	5.232	375	39.4	75	7	60	17.66
c_058_12	0.40	4.525	400	38.9	75	28	60	15.70
c_069_05	0.45	5.405	353	23.9	75	28	65	6.77
c_069_06	0.45	5.405	353	23.9	75	28	65	12.32

References

[1] R.I. Gilbert, G. Ranzi, Time-Dependent Behaviour of Concrete Structures, Taylor & Francis, New York City, NY, 2010.
[2] I. Khan, A. Castel, R.I. Gilbert, Tensile creep and early-age concrete cracking due to restrained shrinkage, Constr. Build. Mater. 149 (2017) 705–715.
[3] Y. Jin, C. Sun, H. Liu, D. Xu, Analysis on the causes of cracking and excessive deflection of long span box girder bridges based on space frame lattice models, Struct 50 (2023) 464–481.
[4] W. Shi, B. Shafei, Z. Liu, B. Phares, Early-age performance of longitudinal bridge joints made with shrinkage-compensating cement concrete, Eng. Struct. 197 (2019), 109391.
[5] H. Chen, D. Li, X. Zhu, W. Zhang, Short-term shrinkage stress in deck concrete of rail-cum-road truss bridge, Case Stud. Constr. Mater. 19 (2023), E02252.
[6] W.J. Weiss, W. Yang, S.P. Shah, Shrinkage cracking of restrained concrete slabs, J. Eng. Mech. 124 (1998) 765–774.
[7] L. Wu, N. Farzadnia, C. Shi, Z. Zhang, H. Wang, Autogenous shrinkage of high performance concrete: a review, Constr. Build. Mater. 149 (2017) 62–75.
[8] E.-I. Tazawa, S. Miyazawa, Influence of cement and admixture on autogenous shrinkage of cement paste, Cem. Concr. Res. 25 (1995) 281–287.
[9] P. Lura, O. Mejlhede Jensen, K. van Breugel, Autogenous shrinkage in high-performance cement paste: an evaluation of basic mechanisms, Cem. Concr. Res. 33 (2003) 223–232.
[10] C. Hua, P. Acker, A. Ehrlacher, Analyses and models of the autogenous shrinkage of hardening cement paste. I. Modelling at macroscopic scale, Cem. Concr. Res. 25 (1995) 1457–1468.
[11] M. Kazemian, B. Shafei, Internal curing capabilities of natural zeolite to improve the hydration of ultra-high performance concrete, Constr. Build. Mater. 340 (2022), 127452.
[12] R. Karim, M. Najimi, B. Shafei, Assessment of transport properties, volume stability, and frost resistance of non-proprietary ultra-high performance concrete, Constr. Build. Mater. 227 (2019), 117031.
[13] Y. Yang, R. Sato, K. Kawai, Autogenous shrinkage of high-strength concrete containing silica fume under drying at early ages, Cem. Concr. Res. 35 (2005) 449–456.

[14] B. Bissonnette, P. Pierre, M. Pigeon, Influence of key parameters on drying shrinkage of cementitious materials, Cem. Concr. Res. 29 (1999) 1655–1662.
[15] M.H. Zhang, C.T. Tam, M.P. Leow, Effect of water-to-cementitious materials ratio and silica fume on the autogenous shrinkage of concrete, Cem. Concr. Res. 33 (2003) 1687–1694.
[16] W. Shi, M. Najimi, B. Shafei, Reinforcement corrosion and transport of water and chloride ions in shrinkage-compensating cement concretes, Cem. Concr. Res. 135 (2020), 106121.
[17] W. Shi, M. Najimi, B. Shafei, Chloride penetration in shrinkage-compensating cement concretes, Cem. Concr. Compos. 113 (2020), 103656.
[18] M. Li, V.C. Li, Behavior of ECC-concrete layered repair system under drying shrinkage conditions, Restor. Build. Monum. 12 (2006) 143–160.
[19] D. Daneshvar, K. Deix, A. Robisson, Effect of casting and curing temperature on the interfacial bond strength of epoxy bonded concretes, Constr. Build. Mater. 307 (2021), 124328.
[20] R.I. Gilbert, Shrinkage cracking in fully restrained concrete members, Acids Struct. J. 89 (1992) 141–149.
[21] A.P. Lampropoulos, S.E. Dritsos, Concrete shrinkage effect on the behavior of RC columns under monotonic and cyclic loading, Constr. Build. Mater. 25 (2011) 1596–1602.
[22] D. Daneshvar, A. Behnood, A. Robisson, Interfacial bond in concrete-to-concrete composites: a review, Constr. Build. Mater. 359 (2022), 129195.
[23] W. Shi, B. Shafei, Bond characteristics between conventional concrete and six high-performance patching materials, Constr. Build. Mater. 308 (2021), 124898.
[24] P. Rossi, J.L. Tailhan, F. Le Maou, L. Gaillet, E. Martin, Basic creep behavior of concretes investigation of the physical mechanisms by using acoustic emission, Cem. Concr. Res. 42 (2012) 61–73.
[25] ACI 209.2R-08, Guide for Modeling and Calculating Shrinkage and Creep in Hardened Concrete, American Concrete Institute, Farmington Hills, MI, 2008.
[26] Z.P. Bazant, S. Baweja, Creep and shrinkage prediction model for analysis and design of concrete structures: Model B3, SP-194, American Concrete Institute, ACI Spec. Publ, Farmington Hills, MI, 2000.
[27] Z.P. Bazant, A.B. Hauggaard, S. Baweja, F. Ulm, Microprestress-solidification theory for concrete creep. I: aging and drying effects, J. Eng. Mech. 123 (1997) 1188–1194.
[28] W. Raphael, E. Zgheib, A. Chateauneuf, Experimental investigations and sensitivity analysis to explain the large creep of concrete deformations in the bridge of Cheviré, Case Stud. Constr. Mater. 9 (2018), E00176.
[29] Z. Pan, B. Li, Z. Lu, Re-evaluation of CEB-FIP 90 prediction models for creep and shrinkage with experimental database, Constr. Build. Mater. 38 (2013) 1022–1030.
[30] D.W. Mokarem, R.E. Weyers, D.S. Lane, Development of a shrinkage performance specifications and prediction model analysis for supplemental cementitious material concrete mixtures, Cem. Concr. Res. 35 (2005) 918–925.
[31] J. Zhu, Y. Wang, Convolutional neural networks for predicting creep and shrinkage of concrete, Constr. Build. Mater. 306 (2021), 124868.
[32] L. Bal, F. Buyle-Bodin, Artificial neural network for predicting drying shrinkage of concrete, Constr. Build. Mater. 38 (2013) 248–254.
[33] M. Liang, Z. Chang, Z. Wan, Y. Gan, E. Schlangen, B. Šavija, Interpretable ensemble-machine-learning models for predicting creep behavior of concrete, Cem. Concr. Compos. 125 (2022), 104295.
[34] L. Liu, X. Wang, H. Chen, C. Wan, M. Zhang, Numerical modeling of drying shrinkage deformation of cement-based composites by coupling multiscale structure model with 3D lattice analyses, Comput. Struct. 178 (2017) 88–104.
[35] A.H. Gandomi, S. Sajedi, B. Kiani, Q. Huang, Genetic programming for experimental big data mining: a case study on concrete creep formulation, Autom. Constr. 70 (2016) 89–97.
[36] AASHTO, LRFD Bridge Design Specifications, American Association of State Highway and Transportation Officials (2012) Washington, DC.
[37] ACI 209, Prediction of creep, shrinkage, and temperature effects in concrete structures, American Concrete Institute, Farmington Hills, MI, 1992.
[38] Comité Européen du Béton, CEB-FIP Model Code, CEB MC90–99 (1999) Lausanne, Switzerland.
[39] European Committee for Standardization, Eurocode 2: Design of Concrete Structures (2004) Brussels, Belgium.
[40] Fédération Internationale du Béton (fib), fib Model Code for Concrete Structures, Ernst & Sohn (2010) Berlin, Germany.
[41] M.H. Hubler, R. Wendner, Z.P. Bazant, *NU-ITI Database of Laboratory Creep and Shrinkage Data* (2008) Northwestern University, Evanston, IL.
[42] Z. Bazant, G.-H. Li, Comprehensive Database on Concrete Creep and Shrinkage (2008) Northwestern University, Evanston, IL.
[43] R. Wendner, M.H. Hubler, Z. Bazant, The B4 model for multi-decade creep and shrinkage prediction, In: Proceedings of the 9th International Conference on Creep, Shrinkage, and Durability Mechanics (2013) Cambridge, MA.
[44] N.J. Gardner, J.W. Zhao, Creep and shrinkage revisited, Acids Mater. J. 90 (3) (1993) 236–246.
[45] JSCE, Standard Specifications for Concrete Structures, Japan Society of Civil Engineers, Tokyo, Japan, 2010.